© 2023. Published by The Company of Biologists Ltd | Journal of Cell Science (2023) 136, jcs260889. doi:10.1242/jcs.260889

RESEARCH ARTICLE

Yck3 casein kinase-mediated phosphorylation determines Ivy1 localization and function at endosomes and the vacuole

Sophie Grziwa[1], Jan-Hannes Schäfer[2], Raffaele Nicastro[3], Annabel Arens[1], Claudio De Virgilio[3], Florian Fröhlich[4,5], Arne Moeller[2,5], Jieqiong Gao[1], Lars Langemeyer[1,5,*] and Christian Ungermann[1,5,*]

ABSTRACT

The *Saccharomyces cerevisiae* casein kinase protein Yck3 is a central regulator at the vacuole that phosphorylates several proteins involved in membrane trafficking. Here, we set out to identify novel substrates of this protein. We found that endogenously tagged Yck3 localized not only at the vacuole, but also on endosomes. To disable Yck3 function, we generated a kinase-deficient mutant and thus identified the I-BAR-protein Ivy1 as a novel Yck3 substrate. Ivy1 localized to both endosomes and vacuoles, and Yck3 controlled this localization. A phosphomimetic Ivy1-SD mutant was found primarily on vacuoles, whereas its non-phosphorylatable SA variant strongly localized to endosomes, similar to what was observed upon deletion of Yck3. *In vitro* analysis revealed that Yck3-mediated phosphorylation strongly promoted Ivy1 recruitment to liposomes carrying the Rab7-like protein Ypt7. Modeling of Ivy1 with Ypt7 identified binding sites for Ypt7 and a positively charged patch, which were both required for Ivy1 localization. Strikingly, Ivy1 mutations in either site resulted in more cells with multilobed vacuoles, suggesting a partial defect in its membrane biogenesis. Our data thus indicate that Yck3-mediated phosphorylation controls both localization and function of Ivy1 in endolysosomal biogenesis.

KEY WORDS: MVB, Endosome, Signaling endosome, Phosphorylation, Ivy1, Yck3, HOPS

INTRODUCTION

The endomembrane system of eukaryotic cells is structured into organelles of distinct identities and function, which are connected by vesicular transport. Within the endolysosomal system, endosomes and lysosomes in mammalian cells, or vacuoles in yeast (herein referring to *Saccharomyces cerevisiae*), are connected to the plasma membrane (PM) and have an important role in controlling the protein composition of the PM and consequently also in metabolic adjustments (Sardana and Emr, 2021; Ballabio and Bonifacino, 2020). Endocytosis of plasma membrane proteins results in the formation of endocytic vesicles, which fuse with the early endosome (EE), where proteins are either sorted into tubules for resorting to the PM or are further directed into intraluminal vesicles (ILVs) with the help of ESCRT proteins (Gruenberg, 2020; Vietri et al., 2020). Consequently, EEs change their shape from a tubular compartment into a multivesicular body (MVB) or late endosome (Klumperman and Raposo, 2014), which then fuses with the lysosome.

EEs are further connected by vesicular transport to the Golgi. Several hydrolases are glycosylated in the Golgi lumen, and then bind to specific receptors, such as the mannose-6-phosphate receptor, and arrive by vesicular transport at EEs, and are further brought to the vacuole lumen (Huotari and Helenius, 2011). An alternative pathway, the adaptor protein complex 3 (AP-3) pathway, transports membrane proteins from the Golgi to the vacuole (Cowles et al., 1997). In yeast, the resulting AP-3 vesicles seem to directly fuse with the vacuole, thus bypassing the EE and MVB (Fig. 1A) (Schoppe et al., 2020; Cowles et al., 1997; Eising et al., 2022).

The organelle identity of EEs, MVB and vacuole in this dynamic system depends on the recruitment and turnover of organelle-specific proteins and lipids. Rab GTPases are landmark proteins, which are controlled by their activating guanine nucleotide exchange factors (GEFs) and GTPase-activating proteins (GAPs) (Borchers et al., 2021). EEs harbor initially Rab5 (Vps21 in yeast), which binds endosomal effectors, such as the CORVET complex, and controls fusion (Zeigerer et al., 2012; Van Der Beek et al., 2019; Borchers et al., 2021). Rab5 is then replaced by Rab7 (note herein Rab5 and Rab7 refer generically to all forms of these proteins), while EEs mature to MVBs (Rink et al., 2005; Poteryaev et al., 2010; Skjeldal et al., 2021; Podinovskaia et al., 2021). In yeast, the Rab7-like Ypt7 then binds the hexameric HOPS complex, which tethers MVBs to vacuoles and promotes fusion. Phosphatidylinositol-phosphates (PIPs) provide a second important organelle-specific marker, which binds to and recruits distinct proteins. At EEs and MVBs, the phosphoinositide 3-kinase (PI3K) Vps34 generates PI3P, which can be further modified to $PI(3,5)P_2$ by the Fab1 complex (PIKfyve in metazoans) (Hasegawa et al., 2017). Both lipids bind specifically to membrane proteins, and either recruit them or change their activity (Ohashi et al., 2019; Hasegawa et al., 2017). It is therefore believed that the dual combination of Rabs and PIPs generates organelle codes, which determine their identity by targeting of membrane proteins to EEs, MVBs, and yeast vacuoles or metazoan lysosomes.

Recently, a subpopulation of endosomes was identified in yeast as having a specific role in signaling (Hatakeyama et al., 2019). They were coined signaling endosomes (SEs) as they are enriched for the target of rapamycin complex 1 (TORC1), a nutrient-regulated kinase complex, which is highly active in the presence of amino acids and thus promotes growth. It was shown that TORC1 recruitment to endosomes depends in part on the EGO complex and its associated Rag GTPases Gtr1 and Gtr2 (the LamTOR–Rag

[1]Osnabrück University, Department of Biology/Chemistry, Biochemistry section, Barbarastrasse 13, 49076 Osnabrück, Germany. [2]Osnabrück University, Department of Biology/Chemistry, Structural Biology, Barbarastrasse 13, 49076 Osnabrück, Germany. [3]Department of Biology, University of Fribourg, Chemin du Musée, CH-1700 Fribourg, Switzerland. [4]Osnabrück University, Department of Biology/Chemistry, Molecular Membrane Biology, Barbarastrasse 13, 49076 Osnabrück, Germany. [5]Osnabrück University, Center of Cellular Nanoanalytic Osnabrück (CellNanOs), Barbarastrasse 13, 49076 Osnabrück, Germany.

*Authors for correspondence (lars.langemeyer@uos.de; cu@uos.de)

J.-H.S., 0000-0001-8163-1629; R.N., 0000-0002-5420-2228; C.D., 0000-0001-8826-4323; F.F., 0000-0001-8307-2189; A.M., 0000-0003-1101-5366; J.G., 0000-0002-5223-6547; L.L., 0000-0002-4309-0910; C.U., 0000-0003-4331-8695

Handling Editor: Giampietro Schiavo
Received 12 December 2022; Accepted 18 May 2023

Journal of Cell Science

Journal of Cell Science (2023) 136, jcs260889. doi:10.1242/jcs.260889

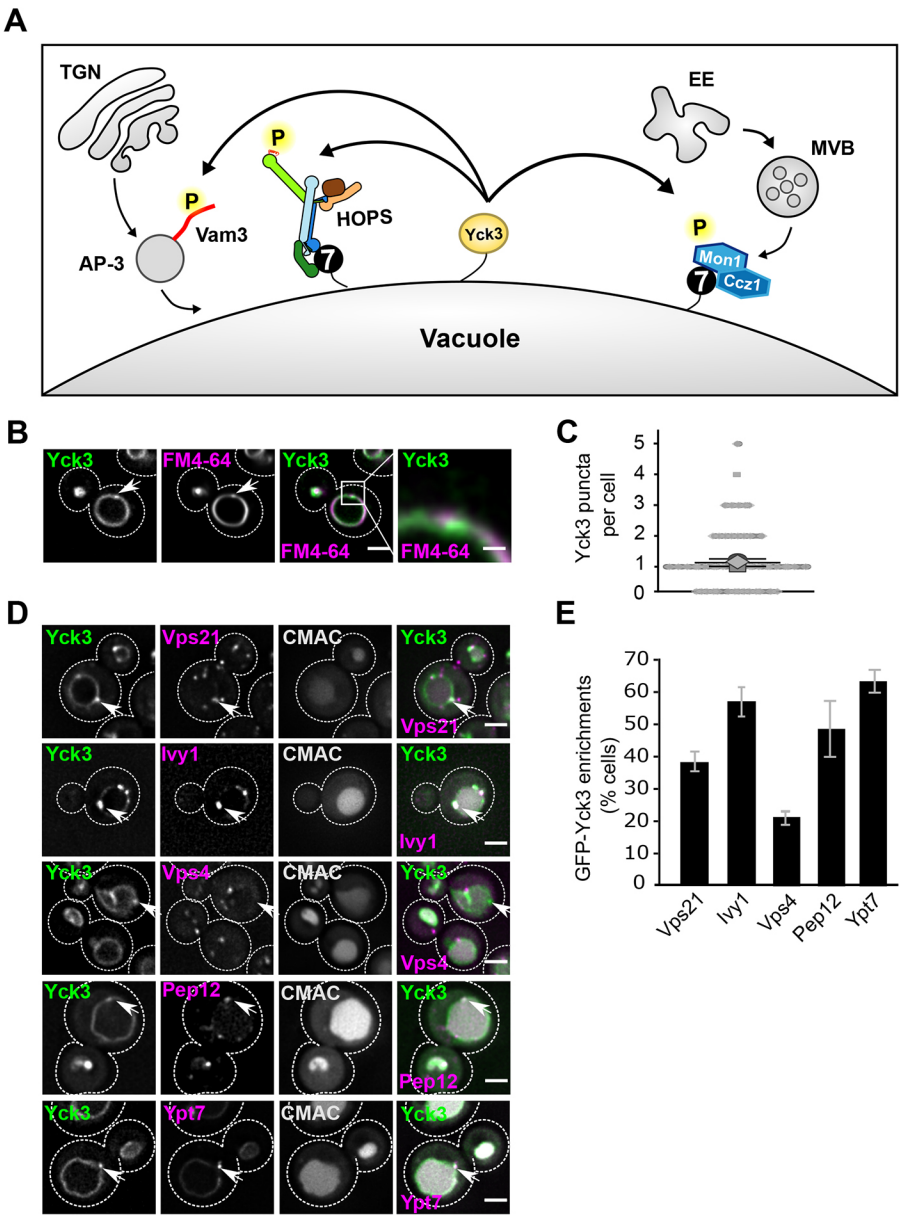

Fig. 1. Yck3 has multiple targets within the endolysosomal pathway. (A) Overview of substrates of Yck3 on the vacuole. See text for details. 7, Ypt7. (B) Localization of endogenously expressed GFP–Yck3. Tagging of Yck3 was performed as described (see Materials and Methods). Vacuolar membranes were stained with FM4-64. Cells were analyzed by fluorescence microscopy and are shown as individual slices. Arrows display Yck3 accumulations. (C) Quantification of the number of Yck3 enrichments per cell. Cells (n>50) were quantified by ImageJ. Error bars represent s.d. of three independent experiments. (D) Localization of different endosomal and vacuolar markers relative to Yck3. Vacuoles were stained with CMAC (see Materials and Methods). Marker proteins mCherry–Vps21, Ivy1–3xmCherry, Vps4–3xHA-mCherry, mCherry–Pep12 or mCherry–Ypt7 were co-expressed in strains encoding endogenous GFP–Yck3. Cells were analyzed by fluorescence microscopy and are shown as individual slices. Arrows display colocalization. (E) Quantification of D. Quantification of percentage of cells showing colocalization of GFP–Yck3 enrichments and the corresponding marker. Cells (n>50) were quantified by ImageJ. Error bars represent s.d. of three independent experiments. Dashed lines highlight edge of cells. Scale bars: 2 µm (main images B; D); 0.4 µm (enlargement in B).

GTPase complex in metazoans), which are also found on SEs (Hatakeyama et al., 2019; Gao et al., 2022; Chen et al., 2021). Intriguingly, TORC1 function seems to be regulated by PI(3,5)P_2 (Takeda et al., 2018; Jin et al., 2014). We recently discovered that TORC1 also phosphorylates Fab1, which then accumulates at SEs (Chen et al., 2021), suggesting that TORC1 can both respond to and control the PIP levels of the SE.

The spatiotemporal analysis of multiple Golgi and endosomal markers suggests that yeast has a minimal endomembrane system, where the trans-Golgi network (TGN) functions as a recycling endosome (Day et al., 2018; Casler and Glick, 2020). It is presently unclear, where SEs fit into this picture. We recently found evidence that SE identity depends both on a functional HOPS complex and the ESCRT machinery, which is present on MVBs (Gao et al., 2022). However, we noticed in that study that any perturbation of the endolysosomal system results in a massive reorganization of the many markers we followed, including TORC1 and the interacting EGO complex (Gao et al., 2022). One of these is the inverted BAR (I-BAR) protein Ivy1, which binds both PI3P and Ypt7, and localizes to both SEs and vacuoles (Lazar et al., 2002; Malia et al., 2018; Numrich et al., 2015; Gao et al., 2022; Ishii et al., 2019). Ivy1 seems to inhibit Fab1 and TORC1 activity, whereas loss of Ivy1 can cause vacuole fragmentation (Malia et al., 2018; Varlakhanova et al., 2018; Numrich et al., 2015). As Ivy1 has a dual localization to SEs and vacuoles, it remained unclear how it is targeted to either organelle and how this targeting is regulated.

Here, we identify Ivy1 as a novel substrate of the casein kinase Yck3. This kinase is sorted to the vacuole via the AP-3 pathway (Sun et al., 2004; Anand et al., 2009) and has so far three identified targets (Fig. 1A) – the HOPS subunit Vps41, the Mon1 subunit of the Ypt7 GEF Mon1–Ccz1 and the vacuolar SNARE Vam3 (LaGrassa and Ungermann, 2005; Cabrera et al., 2010; 2009; Brett et al., 2008; Lawrence et al., 2014). Using endogenously tagged Yck3, we identify that the protein is localized to both vacuoles and, surprisingly, on PI3P- and Ivy1-positive endosomes. As loss of Yck3 resulted in a massive relocalization of Ivy1 to endosomes, we mapped its phosphosites, and used phosphomimetic and non-

Journal of Cell Science (2023) 136, jcs260889. doi:10.1242/jcs.260889

phosphorylatable variants to probe Ivy1 function. We discovered that Ivy1 requires both its positively charged surface and the Ypt7-binding site to bind membranes. Ivy1 phosphorylation strongly enhanced its binding to Ypt7, thus suggesting a mechanism for how Yck3-mediated phosphorylation can affect Ivy1 localization and function.

RESULTS

Yck3 localizes to the vacuole and endosomes

To understand how Yck3 affects endosome and vacuole function (Fig. 1A), we analyzed its localization in detail. In previous studies, N-terminally GFP-tagged Yck3 was overexpressed and found on vacuoles (LaGrassa and Ungermann, 2005). We decided to use N-terminal epitope tagging of Yck3 and to maintain its endogenous expression levels (Gauss et al., 2005). This revealed that Yck3 was present in two populations (Fig. 1B). It was mainly found on vacuoles as shown before (LaGrassa and Ungermann, 2005). In addition, we observed Yck3 in mostly single dot-like structures close to the vacuolar membrane (Fig. 1B,C). To analyze the identity of these dots, we tagged the endosomal Rab5-like Vps21, the endosomal SNARE Pep12 and the ESCRT-IV subunit Vps4 (Fig. 1D) with the red fluorophores mCherry or mKate, and observed clear colocalization with Pep12 (50%) and Vps21 (40%; Fig. 1E). Some structures (20%) were also positive for Vps4 (Fig. 1E). Intriguingly, these dots were also strongly positive for the SE-marker Ivy1 and the Rab7-like Ypt7 protein (some 60%; Fig. 1D,E). This suggests that Yck3 has a dual localization to both vacuoles and endosomes, where it might phosphorylate additional targets.

Yck3 kinase activity is required for the AP-3 pathway and endosomal function

Loss of Yck3 strongly impairs protein trafficking via the AP-3 pathway (Anand et al., 2009; Cabrera et al., 2009). Efficient sorting via the AP-3 pathway requires phosphorylation of the HOPS subunit Vps41, presumably to enable HOPS to capture AP-3 vesicles (Schoppe et al., 2020; Cabrera et al., 2009; 2010). We searched for possible ways to reduce Yck3 function, while maintaining its protein localization, and to this end mutated the predicted Mg^{2+}-binding site within the kinase domain (Fig. 2A). The resulting N155A mutant of Yck3 was still found on vacuoles, although we noticed a reduced number of dots proximal to the vacuole compared to wild-type Yck3 (Fig. 2B). To test activity, we isolated vacuoles, added ATP and monitored Vps41 phosphorylation by band shift analysis on gels (Cabrera et al., 2009). This analysis revealed that the N155A variant was indeed inactive, mimicking the *yck3* deletion (Fig. 2C). In agreement, sorting of a synthetic GFP-tagged AP-3 cargo, consisting of the N-terminal domain of Nyv1 fused to the longer transmembrane domain of the SNARE Snc1 (GNS), resulted in missorting to the plasma membrane, both in *yck3*Δ and $Yck3^{N155A}$ cells (Fig. 2D). To test whether Yck3 had any remaining functional activity, we grew cells in 10-fold dilutions on plates. Cells lacking Yck3 grew slower than wild-type or the *tor1*Δ strain, whereas those expressing $Yck3^{N155A}$ seemed to have residual function, as more growth was observed than for the *yck3* deletion (Fig. 2E). We therefore isolated His-tagged Yck3 wild-type and $Yck3^{N155A}$ from *Escherichia coli* (Fig. 2F) and determined their activity toward isolated Mon1, another known substrate (Lawrence et al., 2014). Using band-shift assays, we revealed that Yck3 wild-type efficiently phosphorylated Mon1, whereas $Yck3^{N155A}$-mediated phosphorylation was delayed (Fig. 2G). This indicates that the $Yck3^{N155A}$ has residual activity *in vitro*.

Kinases have differential activity for their substrates as the binding site adjusts to the substrate (Fulcher and Sapkota, 2020). This was also suggested by our modeling of Yck3 (Fig. 2A, expansion 1). The predicted Yck3 kinase domain (KD) $Yck3^{Y14\text{-}L319}$ showed high confidence values [median predicted local distance difference test (pLDDT)<96], which allows robust interpretation of the model (Fig. S1). To further investigate the effect of the $Yck3^{N155A}$ mutant, the missing ATP and Mg^{2+} were positioned into the point-mutated Yck3 model and optimized for geometric clashes by using the AlphaFill pipeline (Hekkelman et al., 2023). The predicted Mg^{2+}-binding site including the residue N155 forms a salt bridge towards the Mg^{2+} ion within a distance of 2.5 Å. By introducing an alanine at position 155, this salt bridge is lost and the A155–Mg^{2+} distance increases to 4.9 Å (Fig. 2A, expansion 2). Substrate-dependent plasticity of the kinase domain thus might stabilize the bound Mg^{2+} within the ATP-binding site and explain residual *in vitro* activity of $Yck3^{N155A}$.

To understand the consequences of disabling Yck3 activity *in vivo*, we analyzed the endocytic uptake of the lipophilic dye FM4-64 (Fig. 2H). In wild-type cells, the dye primarily stains the vacuole, whereas mutants lacking Yck3 or the ESCRT-IV protein Vps4 also accumulate the dye in membranes proximal to the vacuole. Cells expressing the $Yck3^{N155A}$ variant looked like wild-type. For *vps4*Δ cells, this accumulation corresponds to enlarged class E endosomes (Babst et al., 1998; Adell et al., 2017). When we then combined cells lacking Yck3 or expressing the kinase-deficient $Yck3^{N155A}$ variant with *vps4* mutants, this accumulation of FM4-64 was strongly increased, suggesting that already the impairment of Yck3 function directly affects membrane flux toward the vacuole.

Overall, we conclude that Yck3 requires its full kinase activity for its function in the AP-3 pathway, and controls the function of proteins at endosomes or vacuoles.

Yck3 determines Ivy1 localization

We reasoned that Yck3 function at endosomes and vacuoles depends on interactors. A strongly inactivated kinase, such as $Yck3^{N155A}$, might remain longer in contact with its substrates. To search for interactors or substrates, we isolated Yck3 or $Yck3^{N155A}$ via its GFP tag from the respective cells using the mild detergent digitonin and undertook mass spectrometry to identify any interacting proteins. Mass spectrometry analysis nicely identified Yck3 and some vacuolar proteins, including subunits of the Vtc polyphosphate synthase with low confidence scores (Fig. S2A). This suggests that Yck3 interactions are rather transient and are not stabilized by reducing the kinase activity of Yck3.

To find substrates in an alternative approach, we probed for proteins that colocalized with Yck3 and determined their localization in *yck3*Δ cells. One obvious candidate was Ivy1, which binds both PI3P and Ypt7 (Numrich et al., 2015; Lazar et al., 2002; Gao et al., 2022). It was identified as a low-confidence interactor of Yck3 (Fig. S2A), and strongly colocalized with Yck3 (Fig. 1D). In wild-type cells, GFP-tagged Ivy1 localized to the vacuole and dots (Fig. 3A,B). Strikingly, Ivy1 was completely shifted to the dot-like structure in *yck3*Δ cells (Fig. 3A,B). These structures colocalized strongly with the endosomal marker Vps21 (Fig. 3E,F).

Ivy1 has a central I-BAR domain, which is flanked by seemingly unstructured N- and C-terminal regions (Fig. S2B; Fig. 6A). Several phospho-sites have been identified in these terminal regions (https://www.yeastgenome.org). To determine which of these sites are Yck3 specific, we incubated isolated Ivy1 with wild-type Yck3 and determined phospho-peptides by performing phospho-specific mass spectrometry. Among the many identified sites, a patch

Journal of Cell Science (2023) 136, jcs260889. doi:10.1242/jcs.260889

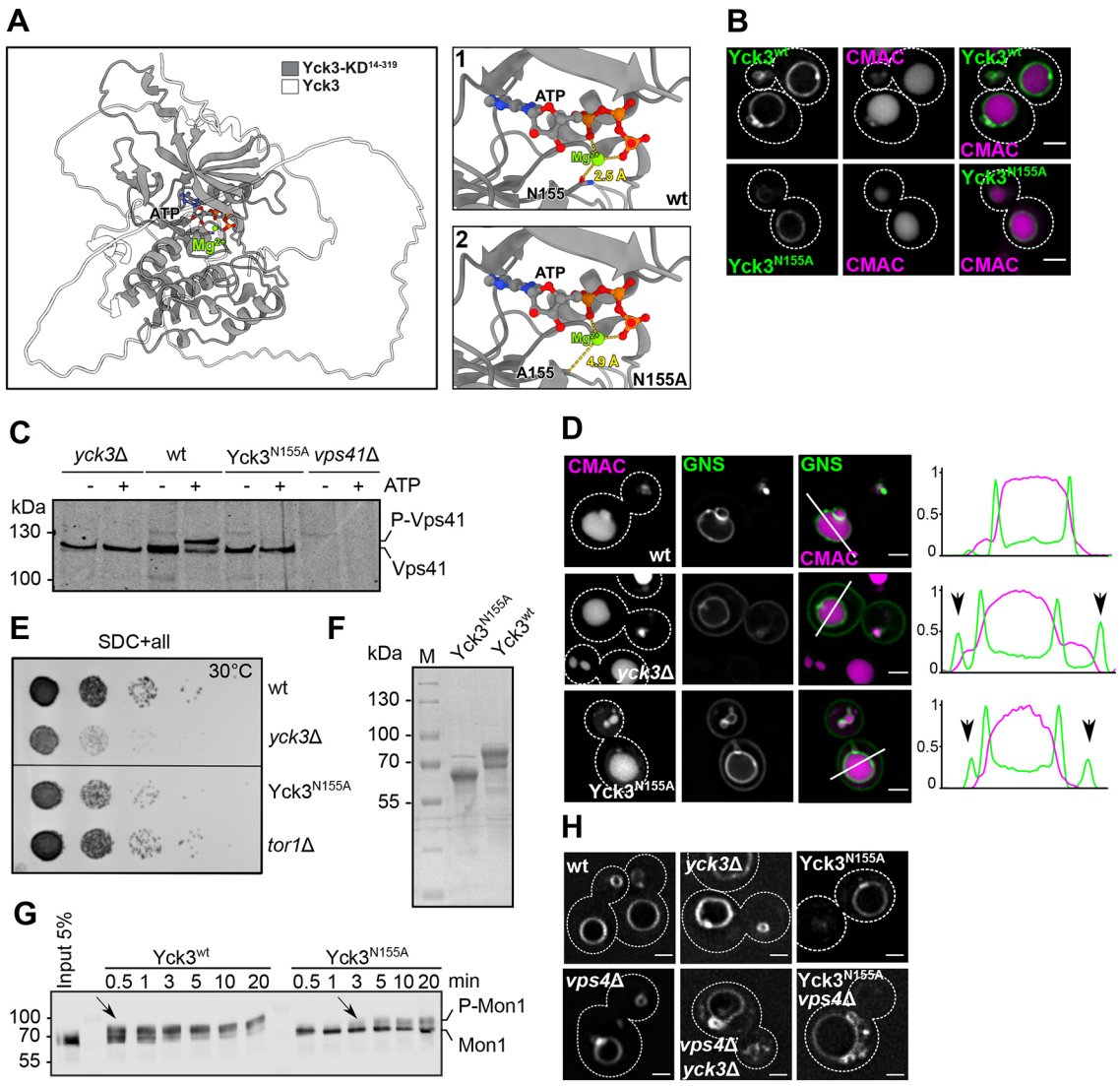

Fig. 2. Analysis of Yck3 kinase function. (A) AlphaFold structure prediction of Yck3 with the kinase domain (KD) in dark gray and the terminal flexible regions represented as transparent cartoons. Enlarged panels focusing on the ATP-binding region of wild-type (1, wt) and Yck3^{N155A} (2) with distance measurements between the catalytic Mg^{2+} (green sphere) and its putative binding partner at position 155. (B) Localization of wild-type Yck3 compared to the catalytically impaired Yck3^{N155A} mutant. Vacuolar membrane was stained with FM4-64 in cells expressing GFP-tagged Yck3 and Yck3^{N155A}. Cells were analyzed by fluorescence microscopy and are shown as individual slices. Arrows display Yck3 accumulations. (C) Vps41 phosphorylation on isolated vacuoles. Vacuoles were isolated by subcellular fractionation and incubated for 40 min without or with ATP. Vacuolar proteins were analyzed on SDS gels, followed by western blotting against Vps41. For details, see Materials and Methods. (D) Analysis of AP-3 sorting. Indicated cells were transformed with a GNS reporter. Cells were analyzed by fluorescence microscopy and are shown as individual slices. Lines show location of indicated line profiles, with arrows on profiles highlighting cells edge. Magenta lines represent CMAC staining, green lines show GFP. (E) Growth analysis of *YCK3* mutants. Cells were sequentially diluted 10-fold, spotted and grown on synthetic minimal medium at 30°C overnight. (F,G) Analysis of Yck3^{N155A} activity. Recombinant Yck3 wild-type and mutant proteins was isolated from *E. coli* (see Materials and Methods). A gel of Coomassie-stained purified Yck3^{N155A} and Yck3^{wt} is shown in F, which was used for determination of *in vitro* kinase activity (G). Wild-type and mutant Yck3 was incubated with purified Mon1–Ccz1 complex as described in the Materials and Methods. At the indicated times, samples were set on ice, and then boiled in SDS-sample buffer. Proteins were analyzed by SDS-PAGE and western blotting against Mon1. (H) Effect of *YCK3* and *VPS4* mutations on endosomal and vacuolar morphology. The indicated strains were incubated with FM4-64 to stain vacuoles. Cells were analyzed by fluorescence microscopy and are shown as individual slices. Outline of cells is shown as dashed line. All images representative of three independent repeats. Dashed lines highlight edge of cells. Scale bars: 2 µm.

of S88, T90, S91 and T92, appeared particularly prominently phosphorylated (Fig. S2B). We therefore mutated these four residues in yeast by CRISPR/Cas9 either to alanine to mimic the non-phosphorylated state (Ivy1^{SA}), or to aspartate (Ivy1^{SD}) to mimic phosphorylated Ivy1. All mutations in Ivy1 generated here and later are listed in Table 1 and did not change expression (Fig. 3D). In agreement with our *yck3*Δ analysis, we observed the Ivy1^{SA} in prominent dots, whereas Ivy1^{SD} was found more on vacuoles, though we also observed occasional dots (Fig. 3A,C). This suggests that our mutations reflect a minimal set of phosphosites targeted by Yck3.

To reveal the identity of Ivy1 dots in wild-type and mutant cells, we analyzed colocalization of Ivy1–GFP with RFP-tagged Vps21 (Fig. 4A), the PI3K subunit Vps34 (Fig. 4B) and the retromer subunit Vps35 (Fig. 4C). As we analyzed in particular dots, which are also apparent in the Ivy1^{SD} mutant, we show here images of such colocalizing structures for all Ivy1 variants. We observed the strongest colocalization of Ivy1^{SA} with retromer (Vps35) and the

Journal of Cell Science (2023) 136, jcs260889. doi:10.1242/jcs.260889

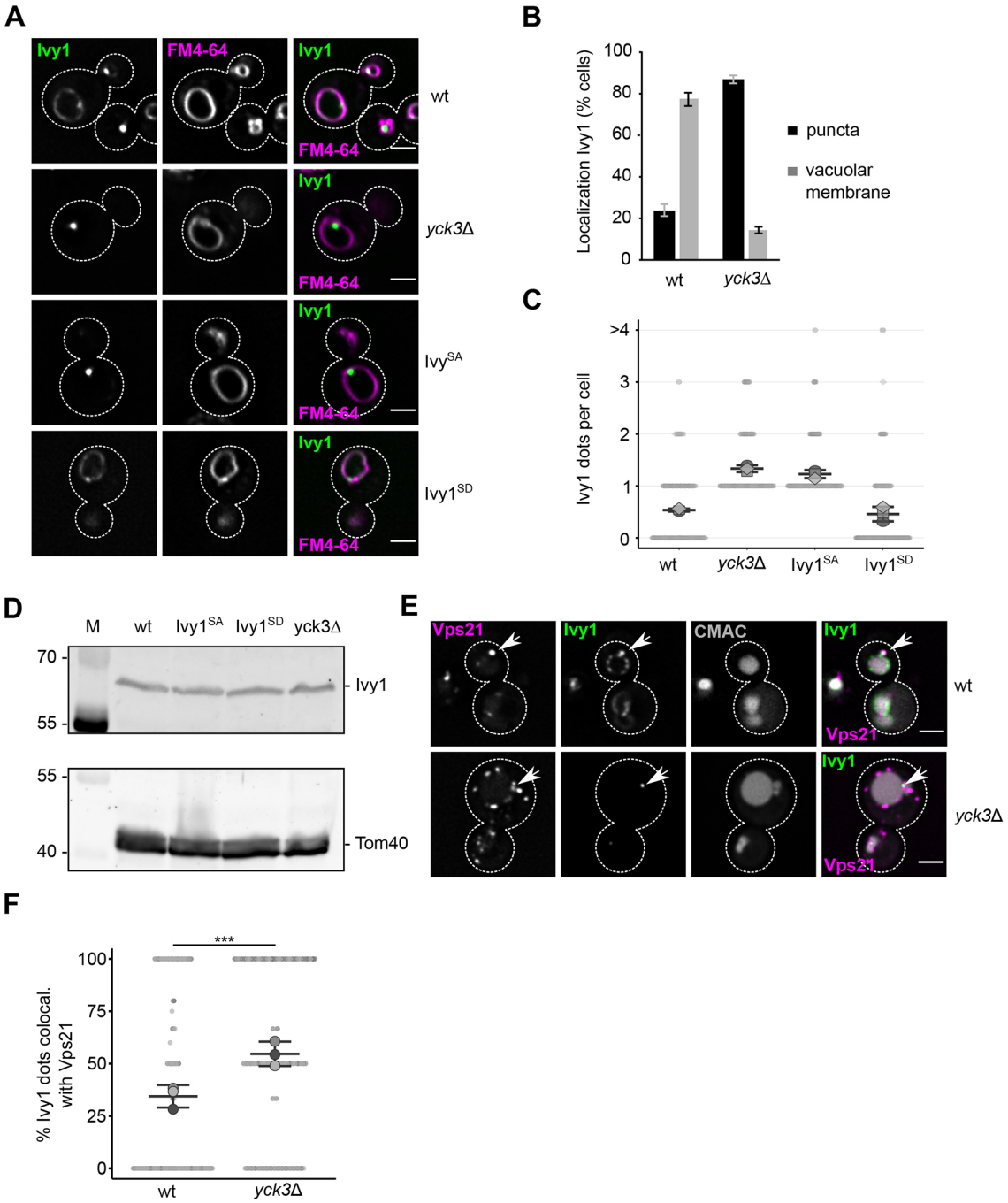

Fig. 3. Ivy1 is a novel substrate of Yck3. (A) Impact of deletions and mutations on Ivy1 localization. Ivy1 was C-terminally tagged with GFP in wild-type (wt) and *yck3*Δ cells. Phospho-mutants of Ivy1 (S88,91A, T90,92A=Ivy1^{SA}; S88,91D, T90,92D=Ivy1^{SD}) were generated by CRISPR/Cas9 in cells expressing Ivy1–GFP. Ivy1–GFP position was analyzed relative to FM4-64-stained vacuoles by fluorescence microscopy, and cells are shown as individual slices. (B) Quantification of Ivy1 localization in wild-type and *yck3*Δ cells. Cells (*n*>50) were quantified by ImageJ. Error bars represent s.d. of three independent experiments. (C) Quantification of the number of Ivy1–GFP dots per cell. Indicated cells (*n*>50) were quantified by ImageJ. Error bars represent s.d. of three independent experiments. (D) Expression levels of Ivy1 in strains used in A. Cells were grown to logarithmic phase and 3 OD_{600} units were harvested. Cells were lysed and protein was TCA precipitated. 50% of samples were analyzed by SDS-PAGE and western blotting using an antibody directed against Ivy1. As loading control, membrane was decorated with an antibody directed against Tom40. (E) Analysis of the Ivy1 structure in wild-type and *yck3*Δ cells. Ivy1 was C-terminally tagged with mGFP, and colocalization with RFP-tagged Vps21 (arrows) was analyzed. Vacuoles were stained with CMAC, and cells were monitored by fluorescence microscopy. Cells are shown as individual slices. (F) Quantification of Ivy1 dots positive for Vps21 colocalization per cell in wild-type and *yck3*Δ cells (*n*>50). Cells were quantified by ImageJ. Error bars represent s.d. of three independent experiments. Dashed lines highlight edge of cells. Scale bars: 2 µm.

PI3K (Vps34) (Fig. 4D), indicating that the non-phosphorylated Ivy1^{SA} dots correspond to endosomes. Ivy1^{SD} instead behaved mostly like wild-type Ivy1, although we observed a reduced amount of Vps34 in Ivy1^{SD}-positive structures. We thus conclude that Yck3-mediated phosphorylation controls the localization of Ivy1 to endosomes and vacuoles.

Journal of Cell Science

Journal of Cell Science (2023) 136, jcs260889. doi:10.1242/jcs.260889

Table 1. Ivy1 mutants used in this study

Mutant	Mutation	Features
Ivy1^{SA}	S88, T90, S91, T92 to alanine (A)	Impaired in Yck3-mediated phosphorylation
Ivy1^{SD}	S88, T90, S91, T92 to aspartate (D)	Phosphomimetic Yck3 sites
Ivy1^{NK-AA}	N289, R292, K293 to alanine (A)	Ypt7-binding site
Ivy1^{CIM}	R220, K227, R228, K229, R231 to alanine (A)	Basic patch (charge independent mutation)

Phosphorylation of Ivy1 affects function

Ivy1 has been implicated as negative regulator of the Fab1 lipid kinase and thus vacuolar membrane homeostasis, as well as an inhibitor of the Gtr1-mediated activation of TORC1 (Varlakhanova et al., 2018; Malia et al., 2018; Ishii et al., 2019). It is possible that both observations are linked, as TORC1 phosphorylates Fab1, which changes its localization to SEs and in turn affects TORC1 activity (Chen et al., 2021). We reasoned that the phosphorylation of Ivy1 could also affect its function. In previous analyses, we observed that an *IVY1* deletion causes a massive expansion of the vacuolar membrane, when combined with a deletion of a subunit of the V-ATPase (Numrich et al., 2015). This might be due to a deficient control of vacuolar membrane homeostasis via TORC1 and Fab1, as TORC1 activity on vacuoles is controlled by the V-ATPase (Zoncu et al., 2011; Hatakeyama et al., 2019), whereas Ivy1 possibly controls Fab1 and TORC1 on endosomes (Malia et al., 2018; Numrich et al., 2015).

To determine which phospho-allele complements Ivy1 function, we here used the same assay. As observed before (Numrich et al., 2015), an *ivy1*Δ *vma16*Δ mutant showed aberrant vacuoles with multiple invaginations by FM4-64 staining, and this phenotype was rescued by introducing Ivy1–GFP from a plasmid (Fig. 5A). We then used the sensitized *vma16*Δ background to test for complementation by our Ivy1 alleles. Either deletion of *YCK3* or introduction of the non-phospho Ivy1^{SA} allele localized Ivy1 to dots, whereas the vacuole appeared like in wild-type cells, suggesting that endosomal Ivy1 is required for this complementation (Fig. 5B,C). In contrast, in cells expressing the vacuole-localized Ivy1^{SD} allele, the maintenance of the vacuolar membrane was as defective as in the *IVY1* deletion background. Cells expressing the kinase-deficient Yck3^{N155A} allele behaved like *yck3*Δ cells, as expected (Fig. 5B,C). This suggests that the complementation of the vacuole expansion phenotype requires endosomal Ivy1.

We then asked whether an artificial confinement of Ivy1^{SD} to endosomes could complement the vacuole morphology defect of the *ivy1*Δ *vma16*Δ mutant phenotype (Fig. 5B). To achieve this, we tagged the endosomal CORVET subunit Vps8 with a chromobody (CB), which efficiently binds to GFP. This approach was previously used to change the localization of Ivy1 to the vacuole (Malia et al., 2018). Importantly, relocalizing Ivy1^{SD} to endosomes restores the defective morphology of vacuoles, which in some cells appeared even more round than in wild-type (Fig. 5D,E). This is consistent with our interpretation that phosphorylation changes the localization of Ivy1, and that the endosomal pool of Ivy1 is required for normal vacuolar morphology.

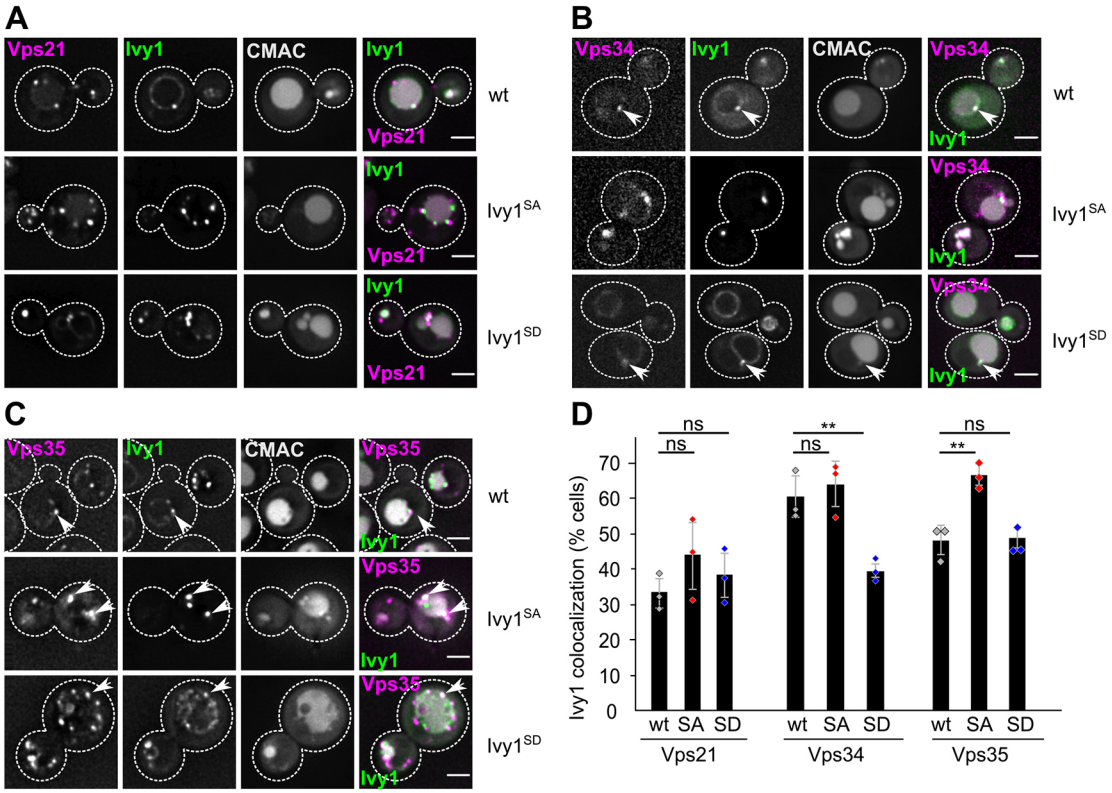

Fig. 4. Localization of Ivy1 mutants to endosomal compartments. (A–C) Localization of wild-type (wt) and phospho-mutants of Ivy1 relative to the endosomal Rab5-like Vps21 (A), the PI3-kinase Vps34 (B) and the retromer subunit Vps35 (C). Ivy1–GFP was expressed in cells encoding mCherry-tagged Vps21, Vps34–mKate and Vps35–mKate. Vacuoles were stained with CMAC. Cells were analyzed by fluorescence microscopy and are shown as individual slices. Arrows indicate colocalization. (D) Quantification of colocalization between Ivy1–GFP and the corresponding marker protein. Cells (n>50) were quantified by ImageJ. Error bars represent s.d. of three independent experiments. Dots display the mean of each independent experiment. *P<0.05; **P<0.01; ns, no significant difference (unpaired two-tailed Student's t-test). Dashed lines highlight edge of cells. Scale bars: 2 µm.

Journal of Cell Science (2023) 136, jcs260889. doi:10.1242/jcs.260889

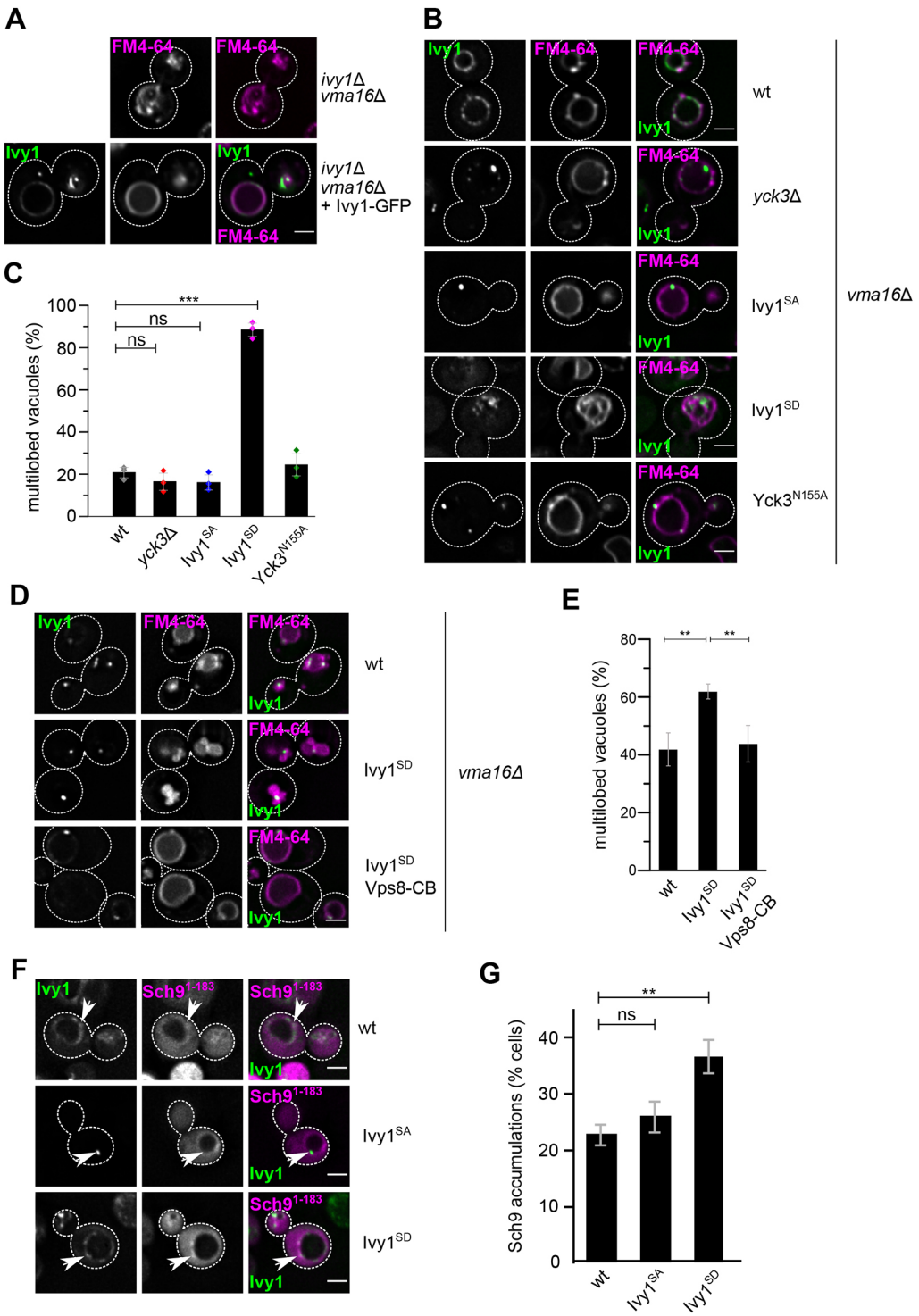

Fig. 5. Endosomal Ivy1 localization is critical for vacuolar membrane integrity. (A) Vacuolar morphology of *ivy1Δ vma16Δ* cells. Cells without or with plasmid expressing Ivy1–GFP were incubated with FM4-64 to stain vacuoles. Cells were analyzed by fluorescence microscopy and are shown as individual slices. (B) Vacuolar morphology of different mutant strains in a *vma16Δ* background. Vacuoles were stained by FM4-64. Cells were analyzed by fluorescence microscopy and are shown as individual slices. (C) Quantification of cells with multilobed vacuoles. Dots display mean of the replicates. Cells (n>50) were quantified by ImageJ. Error bars represent s.d of three independent experiments. (D) Analyzes of vacuole morphology after relocalization of Ivy1^{SD}–GFP using a chromobody (Malia et al., 2018) tagged to endosomal Vps8 directed against GFP in *vma16Δ* cells. Vacuoles were stained by FM4-64. Cells were analyzed by fluorescence microscopy and are shown as individual slices. (E) Quantification of cells (n>50) in D. Error bars represent s.d. of three independent experiments. (F) Localization of a PI(3,5)P_2 reporter in Ivy1 phospho-mutants. The indicated cells expressing Ivy1–GFP and mCherry-tagged Sch9$^{1-183}$ were analyzed by fluorescence microscopy and are shown as individual slices. Arrows indicate colocalization. (G) Quantification of Sch9 accumulations in different Ivy1 cells. Cells (n>50) were quantified by ImageJ. Error bars represent s.d. of three independent experiments. Dots display the mean of each independent experiment. *P<0.05; **P<0.01; ns, no significant difference (unpaired two-tailed Student's t-test). Dashed lines highlight edge of cells. Scale bars: 2 µm.

Another possible consequence could be that endosomal Ivy1 would inhibit Fab1 and thus limit the production of PI(3,5)P_2. We previously established the N-terminal fragment of the TORC1 substrate Sch9$^{1-183}$ as a sensor of the pool of PI(3,5)P_2 (Chen et al., 2021). We used the same assay to monitor RFP-tagged Sch9$^{1-183}$, and observed more Sch9 accumulations in cells expressing the vacuole-localized Ivy1^{SD} (Fig. 5F,G). This observation suggests an alteration in the generation of PI(3,5)P_2, which would be consistent with a role for Ivy1 in modulating Fab1 activity at signaling endosomes.

Phosphorylation promotes Ypt7-dependent membrane binding of Ivy1

Ivy1 has at least two identified membrane-binding sites, to PI3P and to Ypt7 (Lazar et al., 2002; Numrich et al., 2015). To understand how phosphorylation could affect binding of Ivy1 to membranes and Ypt7, we turned to *in silico* modeling using AlphaFold Multimer. Ivy1 has a predicted I-BAR domain flanked by putative disordered regions (Fig. 6A, Fig. S2B). The protein was modelled as a dimer (Fig. 6B,C), similar to other I-BAR domain containing proteins (Nepal et al., 2021). The structure prediction indicates the

Journal of Cell Science (2023) 136, jcs260889. doi:10.1242/jcs.260889

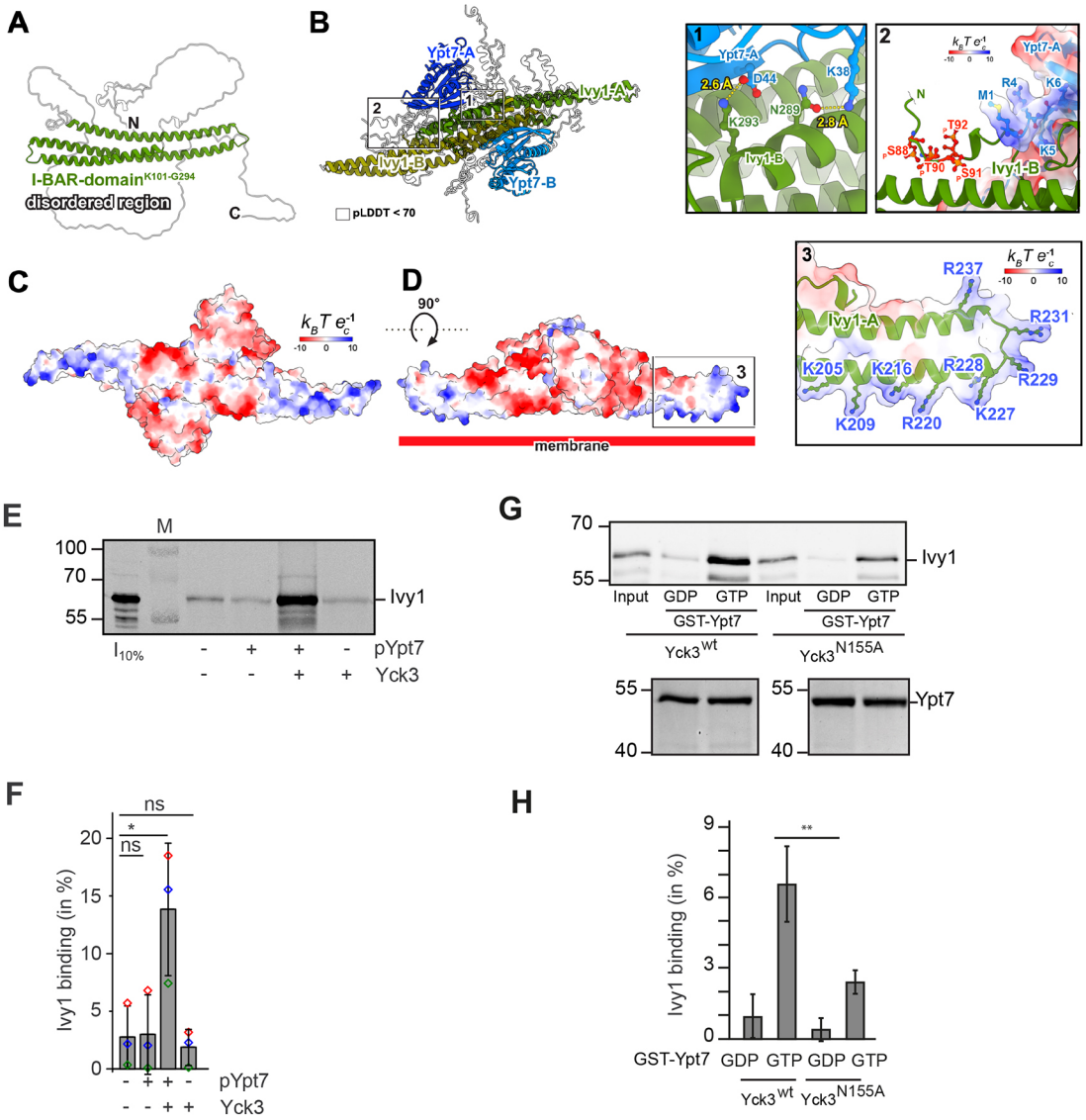

Fig. 6. A heterotetrametric complex of Ivy1 and Ypt7. (A) AlphaFold prediction of Ivy1 reveals a coiled-coil structure covering the putative I-BAR domain (K101-G294, green) and terminal disordered regions (gray). The primary sequence of Ivy1 (B) highlights the putative I-BAR-domain (green) and the phospho-sites S88, T90, S91, T92 (red). The binding site shown in panel (1) involves ionic interactions from Ypt7^{D44} with Ivy1^{K292} and Ypt7^{K38} with Ivy1^{N289}. Panel (2) highlights phospho-sites within the N-terminal region of Ivy1 near the positive electrostatic patch of the Ypt7 N-terminus. (C) Multimeric modeling of Ivy1 and Ypt7 suggests a heterotetrametric C2 symmetric complex with Ypt7 in blue and Ivy1 in green. Low-confidence regions are shown in gray (pLDDT<70). (D) Analysis of the electrostatic surface potential suggests a strong positive patch within the outward-stretching regions within the I-BAR domains of Ivy1 and a positive core region of the complex. The enlarged panel (3) highlights lysine and arginine residues that might facilitate interaction with the membrane. Residues with pLDDT<70 were excluded from the analysis of the surface potential within ChimeraX. (E) Membrane association of Ivy1 with liposomes bearing prenylated Ypt7. Ivy1 was incubated with or without phosphorylation by Yck3 and probed for interaction with Ypt7 (see Materials and Methods for details). Liposomes were incubated with Ivy1 at 4°C for 1 h, added to a sucrose gradient and floated. The top fraction containing liposomes and associated proteins was collected, proteins were TCA-precipitated, and analyzed by western blotting against Ivy1. M, marker; pYpt7, prenylated Ypt7. Molecular mass markers are shown to the right. (F) Quantification of Ivy1 membrane binding as shown in E. Error bars depict s.d. of three independent experiments; colored dots indicate mean of each single experiment. (G) GST–Ypt7 pulldown of Ivy1. Ivy1 was incubated with either Yck3^{wt} or Yck3^{N155A} in presence of ATP. Afterwards it was incubated with immobilized GST–Ypt7 either loaded with GDP or GTP. Bound protein was eluted, and 0.5% of input and 20% of elution fraction was analyzed by SDS-PAGE and western blot using an antibody directed against Ivy1. As a loading control, GSH beads were boiled after EDTA elution and 1% of bound GST–Rab was analyzed on SDS-PAGE by Coomassie staining. (H) Quantification of Ivy1 bound to GST–Ypt7 as shown in G. Three independent experiments were quantified using ImageJ. Signal was normalized to input. Error bars depict s.d. of three independent experiments. *P<0.05; **P<0.01; ns, no significant difference (unpaired two-tailed Student's t-test).

formation of pseudo-C2 symmetric dimers with two putative Ypt7-binding patches flanking the elongated complementing I-BAR domains (Fig. 6B). The resulting complex corresponds to a heterotetramer with two-by-two stoichiometry (Fig. 6B,C).

When modelled with Ypt7, we identified with high confidence an interface that was identical to the Ypt7 binding site previously determined by mutagenesis (Fig. 6B, inset 1) (Malia et al., 2018). The identified Ivy1 residues K293 and N289 likely interact with D44 and K38 of Ypt7 switch I (Fig. 6B, inset 1). Similarly, we searched for a possible membrane binding site, possibly to PI3P or other negatively charged lipids. By analyzing the electrostatic surface potential of the Ivy1-Ypt7 model, we identified a basic patch

Journal of Cell Science (2023) 136, jcs260889. doi:10.1242/jcs.260889

within the I-BAR domain of Ivy1 (Fig. 6C,D). Based on this prediction, we propose the residues K205, K209, K216, R220, K227, R228, K229, R231 and R237 to be responsible for binding to negatively charged membrane lipids (Fig. 6D, inset 3). Intriguingly, the charge distribution of the predicted membrane interface of the entire Ivy1-Ypt7 complex suggests that Ivy1 could deform membranes (Fig. 6D). Ivy1 might thus bind negatively charged phospholipids such as phosphatidylserine or PI(3)P, and form multimers via its I-BAR domain as suggested from previous *in vitro* assays using purified Ivy1 on giant unilamellar vesicles (Numrich et al., 2015). This may cause negative curvature on membranes comparable to other I-BAR proteins (Linkner et al., 2014), though we have currently no functional evidence for this.

We then used our model to analyze the influence of the phospho-sites on the observed preferred binding of Ivy1 to membranes. Modeling of the corresponding residues relative to the I-BAR domain revealed that their phosphorylation would not impair, but rather favor Ypt7 binding (Fig. 6B, inset 2). Our model suggests that phosphorylation of Ivy1 favors the formation of a larger interface due to the positive surface potential within the N-terminal region of Ypt7 and subsequent re-positioning of the phosphorylated residues in Ivy1 (Fig. 6B, expansion 2).

To test whether Ivy1 binding to Ypt7-coated membranes is affected by phosphorylation, we tested for liposome binding. Liposomes were loaded with prenylated Ypt7 using the previously established Ypt7–GDI complex (see Materials and Methods). We preincubated Ivy1 with Yck3 and ATP to promote phosphorylation and added the mixture to liposomes, which were floated in a sucrose gradient. We then probed the top fraction for Ivy1 association by western blotting. Only a very small amount of Ivy1 was found in the top fraction when either Ypt7 or Yck3 were added. However, we observed a clear signal of Ivy1 on membranes after phosphorylation by Yck3 if Ypt7 was present (Fig. 6E,F). As a further control for specificity, we tested whether phosphorylation of Ivy1 by Yck3 modulates its interaction with Ypt7. For this, we incubated purified Ivy1 either with Yck3 or the identified N155A mutant in the presence of ATP and then added each protein separately to GST–Ypt7, loaded with either GDP or GTP. This analysis revealed that Ivy1 strongly interacted with Ypt7–GTP after phosphorylation, whereas the kinase mutant stimulated binding only mildly (Fig. 6G,H). We thus conclude that phosphorylation promotes Ivy1 binding to Ypt7.

Mutations in binding and phospho-sites affect Ivy1 function

We previously showed that Ivy1 localization to membranes is strongly inhibited when Ypt7 is deleted (Malia et al., 2018; Numrich et al., 2015). To ask whether a lack of phosphorylation might still allow for Ivy1 localization to endosomal dots, we analyzed the localization of GFP-tagged Ivy1 wild-type, Ivy1^{SA}, and Ivy1^{SD} in *ypt7*Δ cells. For Ivy1^{SA}, we still observed dot localization (Fig. 7A,B), suggesting that Ypt7-independent binding of Ivy1 to endosomes might occur prior to its Yck3-mediated phosphorylation. In contrast, Ivy1^{SD} localized like the wild-type protein in the cytosol.

To analyze the role of the identified positive patch (Fig. 6D) and Ypt7-binding site in Ivy1 relative to the phosphorylation sites, we mutated the predicted positive charges in Ivy1 wild-type and Ivy1^{SA}, which both have a more pronounced endosomal pool (Figs 3A, 4A). Strikingly, mutations in the basic patch, called CIM for charge independent mutant (Ivy1^{CIM}), or the Ypt7-binding site (Ivy1$^{NK\text{-}AA}$) resulted in a strong cytosolic localization of Ivy1. This suggests that Ypt7 or membrane binding alone are not sufficient for its localization (Fig. 7C,E). Furthermore, vacuoles were abnormal in cells expressing Ivy1^{CIM}. This was not bypassed by blocking the phosphosites in Ivy1 by also inserting the Ivy1^{SA} mutations (Fig. 7D,E). As Ivy1 affects Fab1 activity, which is linked to activity of the TORC1 complex, we expressed reporter constructs that carried a fragment of Sch9 as a TORC1 substrate and a vacuolar or endosomal targeting segment (Hatakeyama et al., 2019). Testing using these constructs revealed that there were only mild effects on vacuolar (VT) and endosomal (ET) TORC1 activity (Fig. S3A,B). Lack of Ivy1 phosphorylation in either *YCK3* deletion or Ivy1^{SA} led to a slightly decreased VT activity. In contrast, ET activity was increased in a strain harboring Ivy1^{CIM} or Ivy1$^{NK\text{-}AA}$ (Fig. S3A,B). This agrees with our previous interpretation of Ivy1 as a regulator of Fab1 and TORC1 in that loss of Ivy1 from endosomes enhances PI(3,5)P_2 production and in turn enhanced ET activity (Malia et al., 2018; Chen et al., 2021). However, it is also possible that the effect of Ivy1 on Fab1 is more pronounced than the subsequent alteration of TORC1 activity, which would explain the modest effect on TORC1 activity observed here. In combination, our analysis suggests that Ivy1 takes advantage of negatively charged lipids, such as PI3P, as well as Ypt7, for its membrane binding and function, with the latter being strongly dependent on Yck3-mediated phosphorylation.

DISCUSSION

We here identified the I-BAR protein Ivy1 as a novel substrate of the casein kinase Yck3. Yck3 localizes not only to vacuoles, as previously observed, but also endosomes, and here in particular to the subpopulation of SEs. Using a catalytically impaired mutant, we discovered that a Yck3 mutant affects both Vps41 and Mon1 phosphorylation, although we do not yet know whether Yck3 has a substrate preference. Interestingly, Ivy1 phosphorylation by Yck3 changes its binding preferences for its interactor Ypt7, which consequently might explain how it alters its localization and function (Fig. 7F). It is also possible that, in turn, the binding preference for PI3P is also changed by phosphorylation. As Ivy1 can inhibit Fab1, which in turn regulates TORC1 function via PI(3,5)P_2 production (Chen et al., 2021), Yck3-mediated phosphorylation might finetune signaling and membrane trafficking at endosomes and vacuoles.

The regulation of endosomal and vacuolar biogenesis is still poorly understood. Biogenesis of both organelles largely depends on endocytic cargo flux, amino acid availability and other nutrients, which in turn control activity of lipid and protein kinases, such as the Fab1 kinase and TORC1 (Battaglioni et al., 2022; Hasegawa et al., 2017). Casein kinases are considered promiscuously active, yet are also regulated by interacting proteins and their localization (Fulcher and Sapkota, 2020; Wang et al., 2015). Yeast has four casein kinases – Yck1, Yck2 and Yck3 are C-terminally lipidated (Roth et al., 2006) and localize to the plasma membrane (Yck1 and Yck2) and vacuole (Yck3), whereas Hrr25 is soluble and has multiple targets at the ER and nucleus (Vancura et al., 1994; Fulcher and Sapkota, 2020). Yck3 sorting to vacuoles occurs via the AP-3 pathway (Sun et al., 2004). It was thus surprising that endogenously expressed Yck3 also colocalized with endosomal markers, including Ivy1. As Yck3 is palmitoylated and prenylated, trafficking to an endosome can occur either by retrograde transport from the vacuole (Suzuki et al., 2021) or by sorting of AP-3 vesicles to an endosomal intermediate compartment (Toshima et al., 2014). It is also possible that Yck3 is sorted similarly to Ego1, which is found also on SEs and was predicted to use both the AP-3 and the endocytic pathway (Hatakeyama et al., 2019).

Journal of Cell Science (2023) 136, jcs260889. doi:10.1242/jcs.260889

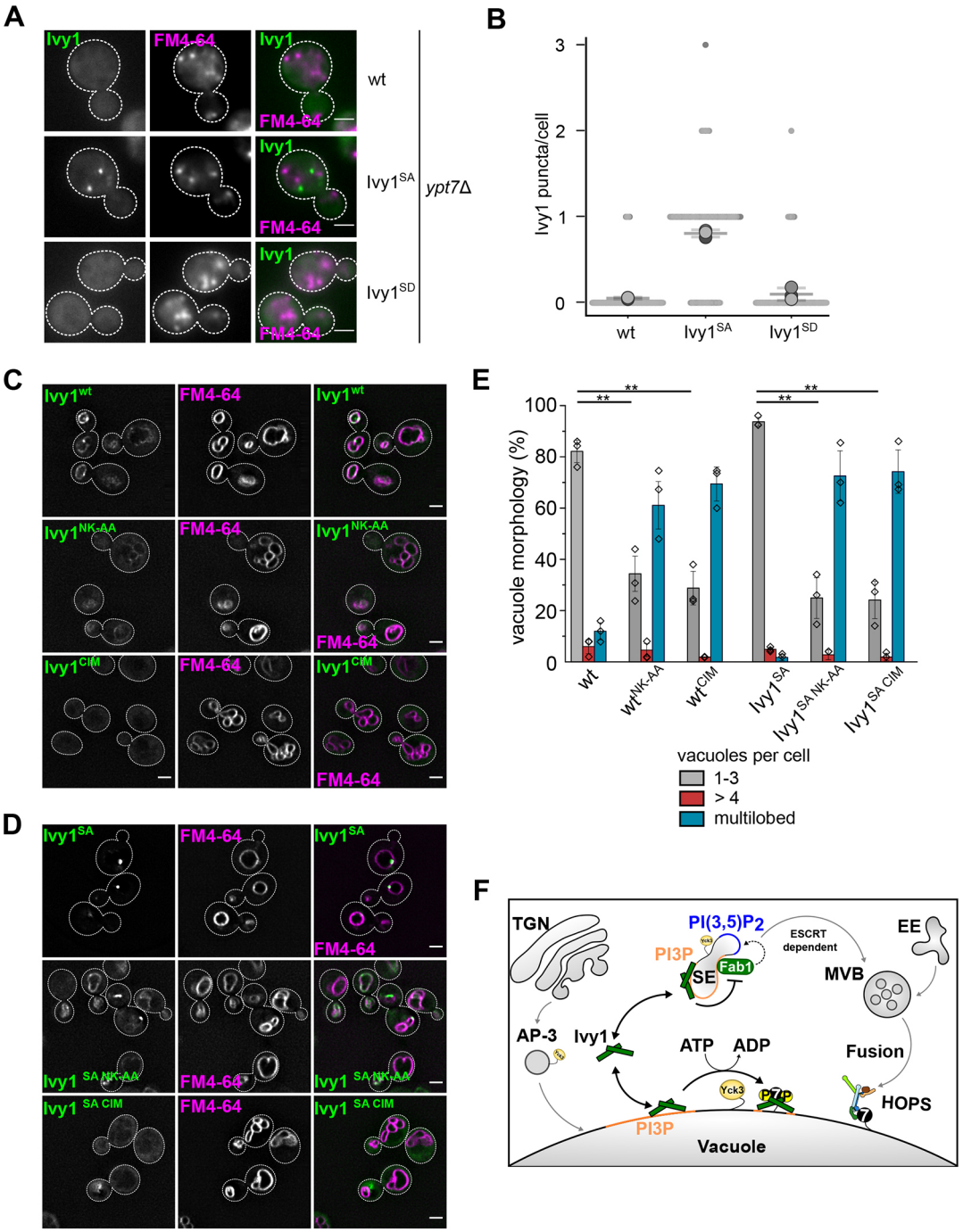

Fig. 7. Effect of Ivy1 mutations on functionality *in vivo*. (A) Localization of Ivy1 phospho-mutants in *ypt7*Δ cells. Vacuoles were stained by FM4-64. Cells expressing the GFP-tagged Ivy1 variants were analyzed by fluorescence microscopy and are shown as individual slices. (B) Quantification of associated Ivy1 puncta per cell. Cells (n>50) were quantified using ImageJ. Error bars represent s.d. of three independent experiments. (C,D) Localization of Ivy1 mutants with mutated Ypt7- and lipid-binding sites. The predicted binding interfaces were mutated in strains expressing Ivy1^{wt}–GFP (C) or Ivy1^{SA}–GFP (D). The Ypt7-binding site was mutated at residues N289A and K293A (Ivy1^{NK-AA}). The predicted lipid binding was mutated at residues R220, K227, R228, K229 and R231 to alanine, resulting in Ivy1^{CIM} (charge independent mutant). Vacuoles were stained with CMAC. Cells were analyzed by fluorescence microscopy and are shown as individual slices. (E) Quantification of vacuole morphology as in C,D. Error bars represent s.d. of three independent experiments. *P<0.05; **P<0.01; ns, no significant difference (unpaired two-tailed Student's t-test). Dashed lines highlight edge of cells. Scale bars: 2 µm. (F) Model of Yck3-mediated control of Ivy1 localization to the vacuole and endosomes.

Ivy1 is unique as an intracellular I-BAR protein, as homologous proteins mainly function at the plasma membrane (Nepal et al., 2021; Salzer et al., 2017). Apart from Ivy1, only I-BARa has been found on intracellular membranes during phagocytosis in *Dictyostelium* (Linkner et al., 2014). We show here that non-phosphorylated Ivy1 preferentially accumulates at SEs. Using the sensitized background of a V-ATPase deletion, we show that the non-phosphorylated Ivy1 is required on endosomes. If Ivy1 is missing or carries the phosphomimetic residues, we observed vacuoles with multiple membrane invaginations in corresponding

mutant cells. We believe that this is caused by deficient regulation of Fab1 at endosomes as the inhibiting endosomal Ivy1 is missing. Because of this, vacuoles seem to have an imbalance in their surface to volume ratio. We are currently testing this hypothesis. Importantly, we could rescue the morphology defect when we artificially targeted the phosphomimetic Ivy1 variant to endosomes, supporting our hypothesis that Ivy1 is needed there.

It is not yet clear where and when Yck3 phosphorylates Ivy1, as both proteins are found both on vacuoles and endosomes, which makes ordering the events challenging. As Ivy1 has two sites through which it can bind to charged lipids, such as PI3P, and Ypt7 (Lazar et al., 2002; Malia et al., 2018; Numrich et al., 2015), membrane targeting could occur via either interaction, or both. In *ypt7*Δ cells, wild-type and the phosphomimetic form of Ivy1 are cytosolic, yet non-phosphorylated Ivy1 is found on endosomes. This suggests that Ivy1 might be initially recruited by charged lipids to endosomes but is rapidly phosphorylated by Yck3 and can then only be stabilized on membranes by interaction with Ypt7. Given that Ivy1 has multiple additional phosphorylation sites, its regulation might be even more complex, and we cannot exclude that also Yck3 modifies additional phosphorylation sites in Ivy1. Additional experiments, including reconstitution, could reveal the order of events and clarify how Ivy1 influences Fab1-mediated $PI(3,5)P_2$ synthesis and turnover on endosomes and vacuoles.

It is intriguing that all other identified Yck3 substrates function as part of the fusion machinery at late endosomes and vacuoles, such as the HOPS subunit Vps41, the Mon1 subunit of the Mon1–Ccz1 complex and Vam3. For Vps41, phosphorylation seems to be required for HOPS function in the AP-3 pathway (Cabrera et al., 2009; 2010), and controls fusion efficiency *in vitro* (Zick and Wickner, 2012; Brett et al., 2008; Hickey et al., 2009), whereas Mon1 phosphorylation rather inhibits its activity (Lawrence et al., 2014; Langemeyer et al., 2020). Vam3 phosphorylation has been reported (Brett et al., 2008), yet neither the corresponding residues have been identified nor is the effect of Vam3 phosphorylation on its function known. It is possible that all phosphorylation events are both substrate and context specific, in that Yck3 interactors and upstream regulators modulate its local activity on vacuoles and endosomes – or along the AP-3 pathway. As our proteomic analysis did not reveal obvious interactors, we believe that regulation could occur through low affinity interactions.

Ivy1 localizes in part to SEs, yet neither its deletion nor mutant proteins lead to apparent changes in TORC1 activity, even though overexpressed Ivy1 can inhibit Fab1 activity (Malia et al., 2018; Numrich et al., 2015). This could be in part due to the fast acquisition of suppressor mutations (Malia et al., 2018), an issue noticed for many yeast deletions (Leeuwen et al., 2020). In contrast, *yck3*Δ cells have a clear growth defect on rapamycin (http://chemogenomics.pharmacy.ubc.ca/fitdb/fitdb2.cgi), possibly due to a defect in AP-3 trafficking and missorting of the EGO complex (Hatakeyama et al., 2019). How Yck3 and in turn then Ivy1 are counter regulated at endosomes and vacuoles and which signals act on Yck3, is an open question. It is possible that endosomal and vacuolar signaling complexes such as TORC1 regulate membrane flux and endosome and vacuole composition in response to their activation by nutrients.

MATERIALS AND METHODS

Yeast strains, plasmids and media

Yeast strains used in this study are listed in Table S1 and plasmids used are listed in Table S2. Where indicated, strains were generated by homologous recombination (Janke et al., 2004). All yeast strains were grown in yeast extract peptone dextrose (YPD) containing 1% yeast extract (Bacto Yeast Extract, Thermo Fisher Scientific, Dreieich, Germany), 2% peptone (Bacto Peptone, Thermo Fisher Scientific) and 2% glucose (Carl Roth, Karlsruhe, Germany). For fluorescence microscopy, yeast strains were grown in synthetic dextrose complete medium (SDC, Thermo Fisher Scientific) overnight, diluted to an optical density at 600 nm (OD_{600}) of 0.2 and grown to logarithmic phase. The antibody against Tom40 (anti-rabbit; used in Fig. 3) was provided by the Neupert laboratory and diluted 1:1000.

CRISPR/Cas9 approach for endogenous mutagenesis

CRISPR/Cas9 was used for generation of genomic point mutants (Generoso et al., 2016). First, a Cas9-containing plasmid was generated with a specific gRNA by Gibson assembly. This plasmid was transformed together with the corresponding homology directed repair fragment (HDR; see primer list in Table S3). After transformation, cells were recovered for 1–2 h in YPD at 30°C and then plated on the corresponding selection plate. Positive clones were selected by sequencing. All plasmids are listed in Table S3.

Light microscopy and image analysis

Cells were grown in SDC medium overnight at 30°C and diluted to an OD_{600}=0.2. When cells reached logarithmic phase, vacuoles were stained with CMAC or FM4-64 (Gao et al., 2022). For CMAC staining, cells were incubated with 0.1 mM 7-amino-4-chloromethylcoumarin (CMAC; Thermo Fisher Scientific) for 10 min. For FM4-64 labeling, cells were incubated with 30 µM of the lipophilic dye FM4-64 (Thermo Fisher Scientific) for 10 min, washed twice in SDC medium, and then incubated for 20 min at 30°C. Images were acquired at a DeltaVision Elite Sytem, which is an Olympus IX-71 inverted microscope equipped with a 100× NA 1.49 objective, a sCMOS camera (PCO), an InsightSSI illumination system and SOftWoRx software (Applied Precision). All images were processed with ImageJ (version 2.3.0). Images were processed to the same intensity levels, and one representative *z*-slice is shown. Colocalization was quantified by counting the percentage of colocalizing dots.

Growth test

Cells were grown overnight in SDC medium, diluted to OD_{600}=0.2, grown to logarithmic phase, and diluted to OD_{600}=0.25. Strains were spotted on SCD plates in serial dilutions (1:10) and incubated at the indicated temperature. All growth tests were performed in triplicates.

Protein expression and purification from *E. coli*

Proteins were expressed in *E. coli* BL21 (DE3) Rosetta cells in presence of the corresponding antibiotics. A preculture was grown overnight in Luria broth (LB) and diluted to an OD_{600}= 0.2. Protein expression was induced by addition of 0.5 mM isopropyl-β-d-thiogalactoside (IPTG) at an OD_{600}= 0.6, and cells were incubated at 16°C overnight. Cells were harvested by centrifugation (4800 ***g***, 10 min, 4°C) and resuspended in buffer containing 300 mM NaCl, 50 mM Tris-HCl pH 7.4, 1 mM PMSF and 0.5× PIC [protease inhibitor mixture; 1× (0.1 mg/ml) leupeptin, 1 mM O-phenanthroline, 0.5 mg/ml pepstatin A, 0.1 mM Pefabloc]. Lysis was performed using the Microfluidizer (Microfluidics Inc.), and the lysate was centrifugated at 25,000 ***g***, 20 min and 4°C. Cleared lysate was added to either prewashed glutathione–Sepharose (GSH) fast flow beads (GE-Healthcare) for GST-tagged fusion proteins or nickel-nitriloacetic acid (Ni-NTA) agarose (Qiagen) for His-tagged proteins. After incubation for 1 h at 4°C on a turning wheel, proteins were eluted at 4°C with buffer (300 mM NaCl, 50 mM Tris-HCl, pH 7.4, 2% glycerol) containing 25 mM glutathione or 300 mM imidazole. Samples were dialyzed against buffer (300 mM NaCl, 50 mM Tris-HCl, pH 7.4, 2% glycerol) overnight. Tags were cleaved off by addition of the SUMO protease (made in house) in an overnight incubation at 4°C with 200 µl of 2 mg/ml SUMO. All proteins were frozen in aliquots at −80°C.

Kinase assay and phospho-site identification by mass spectrometry

The kinase Yck3 was incubated in the presence of 1 mM ATP at a 1:3 ratio together with Ivy1, 2× phosphorylation buffer (300 mM NaCl, 10 mM

Tris-HCl pH 7.4, 10 mM $MgCl_2$ and 0.4 mM EDTA) for 1 h at 30°C. The reaction was stopped by heat inactivation, and an in-solution digest was performed using trypsin and LysC. The digest was performed using the iST Sample Preparation Kit (Preomics, Planegg/Martinsried, Germany). Digested samples were analyzed by mass spectrometry, and RAW data was processed using MaxQuant (Version 1.6.14.0, www.maxquant.org; Cox and Mann, 2008; Cox et al., 2011).

GST Rab pulldown

Assessment of interaction of Ivy1 with GST–Ypt7 was basically performed as before (Langemeyer et al., 2020). In brief, GST–Ypt7 was loaded with either GDP or GTP in the presence of 20 mM EDTA. The loading reaction was stopped by addition of 25 mM $MgCl_2$. 150 µg GST–Ypt7 was then immobilized on 30 µl glutathione–Sepharose by incubation for 1 h at 4°C on a turning wheel. Beads were washed three times using pulldown buffer [50 mM HEPES, 150 mM NaCl, 1 mM $MgCl_2$, 5% (v/v) Glycerol and 0.1% (v/v) Triton X-100]. Next, 50 µg Ivy1 was added, which was incubated with Yck3 and ATP as described for the kinase assay for 1 h at 4°C on a turning wheel. Beads were washed again three times with pulldown buffer, and bound protein was subsequently eluted for 20 min at room temperature in a turning wheel by adding 300 µl elution buffer [50 mM HEPES, pH7.4, 150 mM NaCl, 20 mM EDTA, 5% (v/v) glycerol, 0.1% (v/v) Triton X-100]. Eluted fractions were precipitated with trichloroacetic acid (TCA), and 20% of it was analyzed by SDS-PAGE and western blotting using an antibody directed against Ivy1 (antibody prepared in house; Numrich et al., 2015) and a fluorescently labeled secondary antibody (#SA5-35571, Thermo Fisher Scientific). A 0.5% input was loaded for later quantification. As a loading control for GST–Ypt7, Laemmli buffer was added to the GSH beads after elution of bound protein, and samples were boiled for 5 min at 95°C. 1% of these samples were analyzed by SDS-PAGE and Coomassie Brilliant Blue staining.

Liposome generation

Lipids were purchased from Avanti Polar Lipids, except for ergosterol (Sigma-Aldrich), 1,1′-dioctadecyl-3,3,3′,3′-tetramethylindodicarbocyanine (DiD) (Invitrogen AG) and phosphatidyl-inositol-3-phosphate (PI3P) (Echelon Bioscience). Lipid films including 18 mol% 1-palmitoyl-2-oleoyl-sn-glycero-3-phosphoethanolamine (POPE), 8 mol% ergosterol, 1 mol% diacylglycerol (DAG), 1 mol% DiD and 72 mol% 1-palmitoyl-2-oleoyl-glycero-3-phosphocholine (POPC) were dissolved in buffer containing 50 mM Hepes-NaCl, pH 7.4 and 300 mM NaCl. After ten freeze/thaw cycles in liquid nitrogen, 2 mM liposomes were extruded with a hand extruder (Avanti Polar Lipids) through a polycarbonate filter with a pore size of 400 nm.

Reconstitution of Ivy1 binding to prenylated Ypt7 on liposomes

For the phosphorylation of Ivy1, 1.66 µM Ivy1 was incubated with 0.55 µM Yck3 (3:1 substrate:kinase), 20 mM ATP and 2× phosphorylation buffer (200 mM NaCl, 10 mM Tris-HCl pH 7.5, 10 mM $MgCl_2$, 0.4 mM EDTA, 10% glycerol). The reaction was filled up with water to 30 µl and incubated for 1 h at 30°C while shaking. To load Ypt7 on the liposomes, 0.75 mM liposomes were incubated with 0.75 µM pYpt7-GDI, 1.5 mM EDTA and 200 µM GTP for 15 min at room temperature. The reaction was filled up with buffer containing 50 mM Hepes-NaOH, pH 7.4 and 300 mM NaCl to 100 µl. 3 mM $MgCl_2$ and 0.75 µM phosphorylated Ivy1 were added and filled up with buffer to 150 µl. The samples were incubated for 1 h at 4°C. The solution was mixed with 150 µl 75% sucrose, transferred to SW40 tubes and overlayed with 300 µl 25% sucrose and 150 µl buffer. The tubes were centrifuged in a SW40 Ti (Beckman Coulter) at 100,000 ***g*** for 1 h at 4°C. 200 µl of the top fractions were collected and filled up with 800 µl H_2O. After TCA precipitation, samples were analyzed by western blotting using an antibody directed against Ivy1 (Numrich et al., 2015).

Structure prediction and structure comparison

Predicted models for Yck3 (P39962), Ivy1 (Q04934) and Ypt7 (P32939) were generated with AlphaFold v.2.1.0 (Jumper et al., 2021) in monomer and multimer mode on a local workstation. The provided template date was set to 2020-05-14 for all predictions.

Ivy1 phosphorylation sites were built with PyTMs (Warnecke et al., 2014). The missing ATP and Mg^{2+} were 'transplanted' into Yck3 and optimized using AlphaFill (Hekkelman et al., 2023). All structures were visualized with ChimeraX (Goddard et al., 2018).

Membrane fractionation and band shift analysis of Vps41

Yeast cells were grown overnight at 30°C to an OD_{600}= 1. For the assay, an equivalent of 30 OD_{600} units were pelleted (10 min, room temperature, 2000 ***g***), and treated with 10 mM DTT in 0.1 M Tris-HCl pH 9.4 for 10 min at 30°C. Cells were pelleted at 4600 ***g*** for 2 min at 4°C and resuspended in spheroblasting buffer (0.2× YPD, 50 mM potassium phosphate buffer, pH 7.4, 0.6 M sorbitol). Lyticase (prepared in house) was added (2 mg per 30 OD units), and cells were incubated for 20 min at 30°C. Spheroblasts were centrifuged at 1500 ***g*** for 3 min at 4°C. Supernatant was discarded and spheroblasts were resuspended in 1 ml lysis buffer (0.2 M sorbitol, 50 mM KOAc, 2 mM EDTA, pH 8.0, 20 mM HEPES-KOH, pH 6.8 and 0.125 mg/ml DEAE Dextran). After preincubation on ice for 5 min, spheroblasts were incubated for 2 min at 30°C and subsequently centrifuged at 400 ***g*** for 10 min at 4°C. Supernatant was collected and centrifuged again at 13,000 ***g*** for 15 min at 4°C. The pellet was resuspended in 0% Ficoll and protein concentration was determined. The P13 fraction was diluted to 0.4 mg/ml and 100 µl were incubated with 10× fusion reaction buffer (1.5 M KCl, 5 mM $MnCl_2$, 5 mM $MgCl_2$, 0.2 M sorbitol, 10 mM PIPES-KOH pH 6.8), 0.1 mM CoA and an ATP-regenerating system (0.5 mM ATP, 0.1 mg/ml creatine kinase, 40 mM creatine phosphate, 1 mM PIPES-KOH, pH 6.8, 20 mM sorbitol). After incubation for 45 min at 25°C, samples were centrifuged at 13,000 ***g*** for 15 min at 4°C and analyzed by SDS-PAGE and western blotting. Primary antibodies used were directed against Vps41 (1:3000) and Mon1 (1:3000) (prepared in house).

ET and VT assay to determine TORC1 activity

The ET and VT TORC1 activity assays (including both positive and negative controls) have been previously described in detail (Hatakeyama et al., 2019; Chen et al., 2021; Gao et al., 2022). Accordingly, wild-type and the indicated mutant cells were transformed either with the ET reporter (FYVE-GFP-Sch9$^{C\text{-}term}$) harboring plasmid p3027 (Table S2) or the VT reporter (Sch9$^{C\text{-}term}$-GFP-Pho8$^{N\text{-}term}$) harboring plasmid p2976 (Table S2). 10 ml of cells grown at 30°C on synthetic complete medium (2% glucose, yeast nitrogen base, ammonium sulfate and all amino acids) until mid-log phase were mixed with TCA at a final concentration of 6%. After centrifugation (20,000 ***g*** 10 min, 4°C), the pellet was washed with cold acetone and dried in a speed-vac. The pellet was resuspended in lysis buffer (50 mM Tris-HCl pH 7.5, 5 mM EDTA, 6 M urea and 1% SDS), the amount being proportional to the OD_{600nm} of the original cell culture. Proteins were extracted by agitation in a Precellys machine after addition of glass beads. After the addition of 2× Laemmli buffer (350 mM Tris-HCl pH 6.8, 30% glycerol, 600 mM DTT, 10% SDS, BBF), the mix was boiled at 98°C for 5 min. The analysis was carried out by SDS-PAGE using phospho-specific rabbit anti-Sch9-pThr737 (1:10,000, made in house), goat anti-Sch9 (1:1000, made in house), and mouse anti-GFP (1:1000; 11814460001, Roche) antibodies. Band intensities were quantified using ImageJ software.

Acknowledgements

We thank Siegfried Engelbrecht-Vandré for his help with Yck3 analysis, Zilei Chen and Pedro Carpio Malia for initial Ivy1 analyses, Bill Wickner for plasmids, Ayelén Gonzaléz Montoro and all members of the Ungermann lab for feedback, and Kathrin Auffarth and Angela Perz for expert technical assistance. We also thank Stefan Walter at the mass spectrometry unit at the Center of Cellular Nanoanalytics core facility for support.

Competing interests

The authors declare no competing or financial interests.

Author contributions

Conceptualization: S.G., L.L., C.U.; Methodology: S.G., J.-H.S., R.N., A.A., F.F., J.G.; Software: J.-H.S.; Validation: S.G., J.-H.S., R.N., C.D.V., F.F., A.M.; Formal analysis: S.G., J.-H.S., R.N., A.A., F.F., L.L.; Investigation: S.G., J.-H.S., R.N., A.A.; Resources: S.G., J.-H.S., R.N., A.M.; Data curation: S.G., J.-H.S., R.N., A.A., C.D.V., F.F., A.M., J.G., L.L., C.U.; Writing - original draft: L.L., C.U.; Writing - review &

editing: S.G., J.-H.S., R.N., A.A., C.D.V., F.F., A.M., J.G., L.L., C.U.; Visualization: S.G., J.-H.S., F.F., J.G., L.L., C.U.; Supervision: C.D.V., F.F., A.M., C.U.; Project administration: C.D.V., L.L., C.U.; Funding acquisition: C.D.V., F.F., A.M., C.U.

Funding
This work was funded by the Deutsche Forschungsgemeinschaft (DFG; UN111/10-2 to C.U.), and the SFB 944 (project P11 to CU, project P20 to FF, project P29 to AM), and the Schweizerischer Nationalfonds zur Förderung der Wissenschaftlichen Forschung (Swiss National Science Foundation; 310030_184671 to CDV). J.-H.S. is a fellow of the Friedrich–Ebert Foundation.

Data availability
All relevant data can be found within the article and its supplementary information.

Peer review history
The peer review history is available online at https://journals.biologists.com/jcs/lookup/doi/10.1242/jcs.260889.reviewer-comments.pdf.

References
Adell, M. A. Y., Migliano, S. M., Upadhyayula, S., Bykov, Y. S., Sprenger, S., Pakdel, M., Vogel, G. F., Jih, G., Skillern, W., Behrouzi, R. et al. 2017). Recruitment dynamics of ESCRT-III and Vps4 to endosomes and implications for reverse membrane budding. *Elife* **6**, e31652. doi:10.7554/eLife.31652

Anand, V. C., Daboussi, L., Lorenz, T. C. and Payne, G. S. (2009). Genome-wide analysis of AP-3-dependent protein transport in yeast. *Mol. Biol. Cell* **20**, 1592-1604. doi:10.1091/mbc.e08-08-0819

Babst, M., Wendland, B., Estepa, E. J. and Emr, S. D. (1998). The Vps4p AAA ATPase regulates membrane association of a Vps protein complex required for normal endosome function. *EMBO J.* **17**, 2982-2993. doi:10.1093/emboj/17.11.2982

Ballabio, A. and Bonifacino, J. S. (2020). Lysosomes as dynamic regulators of cell and organismal homeostasis. *Nat. Rev. Mol. Cell Bio.* **21**, 101-118. doi:10.1038/s41580-019-0185-4

Battaglioni, S., Benjamin, D., Wälchli, M., Maier, T. and Hall, M. N. (2022). mTOR substrate phosphorylation in growth control. *Cell* **185**, 1814-1836. doi:10.1016/j.cell.2022.04.013

Borchers, A.-C., Langemeyer, L. and Ungermann, C. (2021). Who's in control? Principles of Rab GTPase activation in endolysosomal membrane trafficking and beyond. *J. Cell Biol.* **220**, e202105120. doi:10.1083/jcb.202105120

Brett, C. L., Plemel, R. L., Lobingier, B. T., Lobinger, B. T., Vignali, M., Fields, S. and Merz, A. J. (2008). Efficient termination of vacuolar Rab GTPase signaling requires coordinated action by a GAP and a protein kinase. *J. Cell Biol.* **182**, 1141-1151. doi:10.1083/jcb.200801001

Cabrera, M., Ostrowicz, C. W., Mari, M., Lagrassa, T. J., Reggiori, F. and Ungermann, C. (2009). Vps41 phosphorylation and the Rab Ypt7 control the targeting of the HOPS complex to endosome–vacuole fusion sites. *Mol. Biol. Cell* **20**, 1937-1948. doi:10.1091/mbc.e08-09-0943

Cabrera, M., Langemeyer, L., Mari, M., Rethmeier, R., Orban, I., Perz, A., Bröcker, C., Griffith, J., Klose, D., Steinhoff, H.-J. et al. (2010). Phosphorylation of a membrane curvature–sensing motif switches function of the HOPS subunit Vps41 in membrane tethering. *J. Cell Biol.* **191**, 845-859. doi:10.1083/jcb.201004092

Casler, J. C. and Glick, B. S. (2020). A microscopy-based kinetic analysis of yeast vacuolar protein sorting. *Elife* **9**, e56844. doi:10.7554/eLife.56844

Chen, Z., Malia, P. C., Hatakeyama, R., Nicastro, R., Hu, Z., Péli-Gulli, M.-P., Gao, J., Nishimura, T., Eskes, E., Stefan, C. J. et al. 2021). TORC1 determines Fab1 lipid kinase function at signaling endosomes and vacuoles. *Curr. Biol.* **31**, 297-309.e8. doi:10.1016/j.cub.2020.10.026

Cowles, C. R., Odorizzi, G., Payne, G. S. and Emr, S. D. (1997). The AP-3 adaptor complex is essential for cargo-selective transport to the yeast vacuole. *Cell* **91**, 109-118. doi:10.1016/S0092-8674(01)80013-1

Cox, J. and Mann, M. (2008). MaxQuant enables high peptide identification rates, individualized p.p.b.-range mass accuracies and proteome-wide protein quantification. *Nat. Biotechnol.* **26**, 1367-1372. doi:10.1038/nbt.1511

Cox, J., Neuhauser, N., Michalski, A., Scheltema, R. A., Olsen, J. V. and Mann, M. (2011). Andromeda: a peptide search engine integrated into the MaxQuant environment. *J. Proteome Res.* **10**, 1794-1805. doi:10.1021/pr101065j

Day, K. J., Casler, J. C. and Glick, B. S. (2018). Budding yeast has a minimal endomembrane system. *Dev. Cell* **44**, 56-72.e4. doi:10.1016/j.devcel.2017.12.014

Eising, S., Esch, B., Wälte, M., Duarte, P. V., Walter, S., Ungermann, C., Bohnert, M. and Fröhlich, F. (2022). A lysosomal biogenesis map reveals the cargo spectrum of yeast vacuolar protein targeting pathways. *J. Cell Biol.* **221**, e202107148. doi:10.1083/jcb.202107148

Fulcher, L. J. and Sapkota, G. P. (2020). Functions and regulation of the serine/threonine protein kinase CK1 family: moving beyond promiscuity. *Biochem. J.* **477**, 4603-4621. doi:10.1042/BCJ20200506doi:10.1042/bcj20200506

Gao, J., Nicastro, R., Péli-Gulli, M.-P., Grziwa, S., Chen, Z., Kurre, R., Piehler, J., Virgilio, C. D., Fröhlich, F. and Ungermann, C. (2022). The HOPS tethering complex is required to maintain signaling endosome identity and TORC1 activity. *J. Cell Biol.* **221**, e202109084. doi:10.1083/jcb.202109084

Gauss, R., Trautwein, M., Sommer, T. and Spang, A. (2005). New modules for the repeated internal and N-terminal epitope tagging of genes in Saccharomyces cerevisiae. *Yeast* **22**, 1-12. doi:10.1002/yea.1187

Generoso, W. C., Gottardi, M., Oreb, M. and Boles, E. (2016). Simplified CRISPR-Cas genome editing for Saccharomyces cerevisiae. *J. Microbiol. Methods* **127**, 203-205. doi:10.1016/j.mimet.2016.06.020

Goddard, T. D., Huang, C. C., Meng, E. C., Pettersen, E. F., Couch, G. S., Morris, J. H. and Ferrin, T. E. (2018). UCSF ChimeraX: meeting modern challenges in visualization and analysis. *Protein Sci.* **27**, 14-25. doi:10.1002/pro.3235

Gruenberg, J. (2020). Life in the lumen: the multivesicular endosome. *Traffic* **21**, 76-93. doi:10.1111/tra.12715

Hasegawa, J., Strunk, B. S. and Weisman, L. S. (2017). PI5P and PI(3,5)P2: minor, but essential phosphoinositides. *Cell Struct. Funct.* **42**, 17003. doi:10.1247/csf.17003

Hatakeyama, R., Péli-Gulli, M.-P., Hu, Z., Jaquenoud, M., Osuna, G. M. G., Sardu, A., Dengjel, J. and Virgilio, C. D. (2019). Spatially distinct pools of TORC1 balance protein homeostasis. *Mol. Cell* **73**, 325-338.e8. doi:10.1016/j.molcel.2018.10.040

Hekkelman, M. L., de Vries, I., Joosten, R. P. and Perrakis, A. (2023). AlphaFill: enriching AlphaFold models with ligands and cofactors. *Nat. Methods* **20**, 205-213. doi:10.1038/s41592-022-01685-y

Hickey, C. M., Stroupe, C. and Wickner, W. (2009). The major role of the Rab Ypt7p in vacuole fusion is supporting HOPS membrane association. *J. Biol. Chem.* **284**, 16118-16125. doi:10.1074/jbc.m109.000737

Huotari, J. and Helenius, A. (2011). Endosome maturation. *EMBO J.* **30**, 3481-3500. doi:10.1038/emboj.2011.286

Ishii, A., Kurokawa, K., Hotta, M., Yoshizaki, S., Kurita, M., Koyama, A., Nakano, A. and Kimura, Y. (2019). Role of Atg8 in the regulation of vacuolar membrane invagination. *Sci. Rep.* **9**, 14828. doi:10.1038/s41598-019-51254-1

Janke, C., Magiera, M. M., Rathfelder, N., Taxis, C., Reber, S., Maekawa, H., Moreno-Borchart, A., Doenges, G., Schwob, E., Schiebel, E. et al. (2004). A versatile toolbox for PCR-based tagging of yeast genes: new fluorescent proteins, more markers and promoter substitution cassettes. *Yeast* **21**, 947-962. doi:10.1002/yea.1142

Jin, N., Mao, K., Jin, Y., Tevzadze, G., Kauffman, E. J., Park, S., Bridges, D., Loewith, R., Saltiel, A. R., Klionsky, D. J. et al. (2014). Roles for PI(3,5)P2 in nutrient sensing through TORC1. *Mol. Biol. Cell* **25**, 1171-1185. doi:10.1091/mbc.e14-01-0021

Jumper, J., Evans, R., Pritzel, A., Green, T., Figurnov, M., Ronneberger, O., Tunyasuvunakool, K., Bates, R., Žídek, A., Potapenko, A. et al. (2021). Highly accurate protein structure prediction with AlphaFold. *Nature* **596**, 583-589. doi:10.1038/s41586-021-03819-2

Klumperman, J. and Raposo, G. (2014). The complex ultrastructure of the endolysosomal system. *Cold Spring Harbor Perspect. Biol.* **6**, a016857. doi:10.1101/cshperspect.a016857

Lagrassa, T. J. and Ungermann, C. (2005). The vacuolar kinase Yck3 maintains organelle fragmentation by regulating the HOPS tethering complex. *J. Cell Biol.* **168**, 401-414. doi:10.1083/jcb.200407141

Langemeyer, L., Borchers, A.-C., Herrmann, E., Füllbrunn, N., Han, Y., Perz, A., Auffarth, K., Kümmel, D. and Ungermann, C. (2020). A conserved and regulated mechanism drives endosomal Rab transition. *Elife* **9**, e56090. doi:10.7554/elife.56090

Lawrence, G., Brown, C. C., Flood, B. A., Karunakaran, S., Cabrera, M., Nordmann, M., Ungermann, C. and Fratti, R. A. (2014). Dynamic association of the PI3P-interacting Mon1-Ccz1 GEF with vacuoles is controlled through its phosphorylation by the type 1 casein kinase Yck3. *Mol. Biol. Cell* **25**, 1608-1619. doi:10.1091/mbc.e13-08-0460

Lazar, T., Scheglmann, D. and Gallwitz, D. (2002). A novel phospholipid-binding protein from the yeast Saccharomyces cerevisiae with dual binding specificities for the transport GTPase Ypt7p and the Sec1-related Vps33p. *Eur. J. Cell Biol.* **81**, 635-646. doi:10.1078/0171-9335-00290

Leeuwen, J., Pons, C., Tan, G., Wang, J. Z., Hou, J., Weile, J., Gebbia, M., Liang, W., Shuteriqi, E., Li, Z. et al. (2020). Systematic analysis of bypass suppression of essential genes. *Mol. Syst. Biol.* **16**, e9828. doi:10.15252/msb.20209828

Linkner, J., Witte, G., Zhao, H., Junemann, A., Nordholz, B., Runge-Wollmann, P., Lappalainen, P. and Faix, J. (2014). The inverse BAR domain protein IBARa drives membrane remodeling to control osmoregulation, phagocytosis and cytokinesis. *J. Cell Sci.* **127**, 1279-1292. doi:10.1242/jcs.140756

Malia, P., Numrich, J., Nishimura, T., Montoro, A. G., Stefan, C. J. and Ungermann, C. (2018). Control of vacuole membrane homeostasis by a resident PI-3,5-kinase inhibitor. *Proc. Natl. Acad. Sci. USA* **115**, 201722517. doi:10.1073/pnas.1722517115

Nepal, B., Sepehri, A. and Lazaridis, T. (2021). Mechanism of negative membrane curvature generation by I-BAR domains. *Structure* **29**, 1440-1452.e4. doi:10.1016/j.str.2021.07.010

Numrich, J., Péli-Gulli, M.-P., Arlt, H., Sardu, A., Griffith, J., Levine, T., Engelbrecht-Vandré, S., Reggiori, F., Virgilio, C. D. and Ungermann, C.

(2015). The I-BAR protein Ivy1 is an effector of the Rab7 GTPase Ypt7 involved in vacuole membrane homeostasis. *J. Cell Sci.* **128**, 2278-2292. doi:10.1242/jcs.164905

Ohashi, Y., Tremel, S. and Williams, R. L. (2019). VPS34 complexes from a structural perspective. *J. Lipid Res.* **60**, 229-241. doi:10.1194/jlr.r089490

Podinovskaia, M., Prescianotto-Baschong, C., Buser, D. P. and Spang, A. (2021). A novel live-cell imaging assay reveals regulation of endosome maturation. *Elife* **10**, e70982. doi:10.7554/elife.70982

Poteryaev, D., Datta, S., Ackema, K., Zerial, M. and Spang, A. (2010). Identification of the switch in early-to-late endosome transition. *Cell* **141**, 497-508. doi:10.1016/j.cell.2010.03.011

Rink, J., Ghigo, E., Kalaidzidis, Y. and Zerial, M. (2005). Rab conversion as a mechanism of progression from early to late endosomes. *Cell* **122**, 735-749. doi:10.1016/j.cell.2005.06.043

Roth, A. F., Wan, J., Bailey, A. O., Sun, B., Kuchar, J. A., Green, W. N., Phinney, B. S., Yates, J. R. and Davis, N. G. (2006). Global analysis of protein palmitoylation in yeast. *Cell* **125**, 1003-1013. doi:10.1016/j.cell.2006.03.042

Salzer, U., Kostan, J. and Djinović-Carugo, K. (2017). Deciphering the BAR code of membrane modulators. *Cell. Mol. Life Sci.* **74**, 2413-2438. doi:10.1007/s00018-017-2478-0

Sardana, R. and Emr, S. D. (2021). Membrane protein quality control mechanisms in the endo-lysosome system. *Trends Cell Biol.* **31**, 269-283. doi:10.1016/j.tcb.2020.11.011

Schoppe, J., Mari, M., Yavavli, E., Auffarth, K., Cabrera, M., Walter, S., Fröhlich, F. and Ungermann, C. (2020). AP–3 vesicle uncoating occurs after HOPS–dependent vacuole tethering. *EMBO J.* **39**, e2020105117. doi:10.15252/embj.2020105117

Skjeldal, F. M., Haugen, L. H., Mateus, D., Frei, D. M., Rødseth, A. V., Hu, X. and Bakke, O. (2021). De novo formation of early endosomes during Rab5 to Rab7 transition. *J. Cell Sci.* **134**, jcs254185. doi:10.1242/jcs.254185

Sun, B., Chen, L., Cao, W., Roth, A. F. and Davis, N. G. (2004). The yeast casein kinase Yck3p is palmitoylated, then sorted to the vacuolar membrane with AP-3-dependent recognition of a YXXPhi adaptin sorting signal. *Mol. Biol. Cell* **15**, 1397-1406. doi:10.1091/mbc.e03-09-0682

Suzuki, S. W., Oishi, A., Nikulin, N., Jorgensen, J. R., Baile, M. G. and Emr, S. D. (2021). A PX-BAR protein Mvp1/SNX8 and a dynamin-like GTPase Vps1 drive endosomal recycling. *Elife* **10**, e69883. doi:10.7554/elife.69883

Takeda, E., Jin, N., Itakura, E., Kira, S., Kamada, Y., Weisman, L. S., Noda, T. and Matsuura, A. (2018). Vacuole-mediated selective regulation of TORC1-Sch9 signaling following oxidative stress. *Mol. Biol. Cell* **29**, 510-522. doi:10.1091/mbc.e17-09-0553

Toshima, J. Y., Nishinoaki, S., Sato, Y., Yamamoto, W., Furukawa, D., Siekhaus, D. E., Sawaguchi, A. and Toshima, J. (2014). Bifurcation of the endocytic pathway into Rab5-dependent and -independent transport to the vacuole. *Nat. Commun.* **5**, 3498. doi:10.1038/ncomms4498

Van Der Beek, J., Jonker, C., Van Der Welle, R., Liv, N. and Klumperman, J. (2019). CORVET, CHEVI and HOPS – multisubunit tethers of the endo-lysosomal system in health and disease. *J. Cell Sci.* **132**, jcs189134. doi:10.1242/jcs.189134

Vancura, A., Sessler, A., Leichus, B. and Kuret, J. (1994). A prenylation motif is required for plasma membrane localization and biochemical function of casein kinase I in budding yeast. *J. Biol. Chem.* **269**, 19271-19278. doi:10.1016/S0021-9258(17)32163-4

Varlakhanova, N. V., Tornabene, B. A. and Ford, M. G. J. (2018). Ivy1 is a negative regulator of Gtr-dependent TORC1 activation. *J. Cell Sci.* **131**, jcs218305. doi:10.1242/jcs.218305

Vietri, M., Radulovic, M. and Stenmark, H. (2020). The many functions of ESCRTs. *Nat. Rev. Mol. Cell Bio.* **21**, 25-42. doi:10.1038/s41580-019-0177-4

Wang, J., Davis, S., Menon, S., Zhang, J., Ding, J., Cervantes, S., Miller, E., Jiang, Y. and Ferro-Novick, S. (2015). Ypt1/Rab1 regulates Hrr25/CK1δ kinase activity in ER–Golgi traffic and macroautophagy. *J. Cell Biol.* **210**, 273-285. doi:10.1083/jcb.201408075

Warnecke, A., Sandalova, T., Achour, A. and Harris, R. A. (2014). PyTMs: a useful PyMOL plugin for modeling common post-translational modifications. *BMC Bioinformatics* **15**, 370. doi:10.1186/preaccept-1977987350137477

Zeigerer, A., Gilleron, J., Bogorad, R. L., Marsico, G., Nonaka, H., Seifert, S., Epstein-Barash, H., Kuchimanchi, S., Peng, C. G., Ruda, V. M. et al. (2012). Rab5 is necessary for the biogenesis of the endolysosomal system in vivo. *Nature* **485**, 465-470. doi:10.1038/nature11133

Zick, M. and Wickner, W. (2012). Phosphorylation of the effector complex HOPS by the vacuolar kinase Yck3p confers Rab nucleotide specificity for vacuole docking and fusion. *Mol. Biol. Cell* **23**, 3429-3437. doi:10.1091/mbc.e12-04-0279

Zoncu, R., Bar-Peled, L., Efeyan, A., Wang, S., Sancak, Y. and Sabatini, D. M. (2011). mTORC1 senses lysosomal amino acids through an inside-out mechanism that requires the vacuolar H^+-ATPase. *Science* **334**, 678-683. doi:10.1126/science.1207056